

Exploring the expression patterns of palmitoylating and de-palmitoylating enzymes in the mouse brain using the curated RNA-seq database BrainPalmSeq

Authors: Wild, AR¹; Hogg, PW¹; Flibotte, S²; Nasser, G¹; Hollman, R¹; Abazari, D¹; Haas, K¹ and Bamji, SX¹

Affiliations:

1 Department of Cellular and Physiological Sciences, Life Sciences Institute and Djavad Mowafaghian Centre for Brain Health, University of British Columbia

2 Life Sciences Institute Bioinformatics Facility, University of British Columbia

Correspondence:

Shernaz Bamji, Ph.D.

Department of Cellular and Physiological Sciences

Life Sciences Institute,

Djavad Mowafaghian Centre for Brain Health

University of British Columbia

2350 Health Sciences Mall

Vancouver, B.C., V6T 1Z3

Off: 604-822-4746

Abstract

Protein *S*-palmitoylation is a reversible post-translational lipid modification that plays a critical role in neuronal development and plasticity, while dysregulated *S*-palmitoylation underlies a number of severe neurological disorders. Dynamic *S*-palmitoylation is regulated by a large family of ZDHHC palmitoylating enzymes, their accessory proteins, and a small number of known de-palmitoylating enzymes. Here, we curated and analyzed expression data for the proteins that regulate *S*-palmitoylation from publicly available RNAseq datasets, providing a comprehensive overview of their distribution in the mouse nervous system. We developed a web-tool that enables interactive visualization of the expression patterns for these proteins in the nervous system (<http://brainpalmseq.med.ubc.ca/>), and explored this resource to find region and cell-type specific expression patterns that give insight into the function of palmitoylating and de-palmitoylating enzymes in the brain and neurological disorders. We found coordinated expression of ZDHHC enzymes with their accessory proteins, de-palmitoylating enzymes and other brain-expressed genes that included an enrichment of *S*-palmitoylation substrates. Finally, we utilized ZDHHC expression patterns to predict and validate palmitoylating enzyme-substrate interactions.

Introduction

Protein *S*-palmitoylation is a post-translational lipid modification that mediates dynamic changes in protein stability, function, and membrane localization. *S*-palmitoylation is defined as the reversible formation of a cysteine residue thioester bond with the fatty acid palmitate, and is the most prevalent post-translational lipid modification in the brain. Dynamic changes in *S*-palmitoylation are critical for neuronal development and synaptic plasticity (Fukata et al., 2013; Fukata and Fukata, 2010; Globa and Bamji, 2017; Matt et al., 2019), oligodendrocyte differentiation and myelination (Ma et al., 2021; Schneider et al., 2005), and astrocyte proliferation (Yuan et al., 2021). Furthermore, numerous neurological and psychiatric diseases have now been attributed to mutations in the genes encoding palmitoylating and de-palmitoylating enzymes, including schizophrenia, intellectual disability and CLN1 disease (Mukai et al., 2004; Nita et al., 2016; Raymond et al., 2007), underscoring the importance of proper regulation of *S*-palmitoylation for normal brain function.

S-Palmitoylation is catalyzed by a family of ZDHHC enzymes that share a consensus 'Asp-His-His-Cys' catalytic domain. These enzymes are structurally heterogeneous multi-pass transmembrane proteins that localize to a variety of subcellular compartments, including the Golgi apparatus, endoplasmic reticulum (ER), recycling endosomes and the plasma membrane (Globa and Bamji, 2017). The ZDHHC enzymes are known to associate with accessory proteins that regulate their stability, activity,

and trafficking (Salaun et al., 2020). Several de-palmitoylating enzymes have also been identified that are divided into three classes: the acyl-protein thioesterases that shuttle between the Golgi and cytosol (APTs; Vartak et al., 2014), the predominantly lysosomal palmitoyl-protein thioesterases (PPTs; Koster and Yoshii, 2019) and the more recently discovered α/β hydrolase domain-containing proteins (ABHDs; Lin and Conibear, 2015). Unlike other post-translational modifications, palmitoylation lacks a consensus substrate amino sequence. To date there is no unifying theory to explain how substrate recognition is achieved, with contrasting reports of substrate interactions being both promiscuous and specific (Malgapo and Linder, 2021). Currently these interactions are thought to be governed by the subcellular targeting of ZDHHCs enzymes and the presence of protein-protein interacting motifs within the ZDHHC N- and C-termini, which are highly diverse among the ZDHHC enzymes (Rana et al., 2018). Differential gene expression can also have a profound influence on protein interactions and may play a role in the coordination of S-palmitoylation in the brain. However, a detailed overview and analysis of the precise cellular and regional expression patterns of the palmitoylating and de-palmitoylating enzymes has not yet been described, and as such, little is known about how this expression is coordinated in the nervous system.

Recent advances in single-cell RNA sequencing (scRNAseq) techniques have enabled the classification of neuronal and non-neuronal cell types in unprecedented detail, providing a better understanding of cellular diversity and function in the nervous system, while also providing a means to study the expression patterns of individual genes across an ever-expanding range of brain regions and cellular classifications. Here, we capitalized on the recent surge in RNAseq publications characterizing regional and cellular transcriptomics of the mouse nervous system. We curated and analyzed expression data from a number of publicly available RNAseq mouse datasets to generate a detailed analysis of the expression patterns of the genes associated with S-palmitoylation in the mouse brain. Furthermore, we present an interactive web tool that allows user-driven interrogation of the expression patterns of palmitoylating and de-palmitoylating enzymes from numerous collated studies across a variety of brain regions and cell types (<http://brainpalmseq.med.ubc.ca/>). We demonstrate the utility of this resource by detailing the considerable cell-type and regional heterogeneity in expression patterns of these enzyme families and their accessory proteins, revealing numerous cell-type enrichments and co-expression patterns that allowed us to generate and test hypotheses about palmitoylating enzyme-substrate interactions.

Results

BrainPalmSeq: an interactive database to search palmitoylating and depalmitoylating enzyme expression in the mouse brain

The recent development of scRNAseq has revolutionized our understanding of the complex transcriptional diversity of neuronal and non-neuronal cell types in the brain. We found however, there were several barriers to the easy access for much of this data, with no single resource available to evaluate multi-study expression datasets. Data can also be difficult to access when studies are not accompanied by an interactive online web viewer, while datasets that do have a web viewer employ diverse interfaces that are often complex, particularly for large scRNAseq datasets. Furthermore, the differing study-specific analysis pipelines, as well as the variety of data presentation formats in web viewers including heatmaps, bar charts, tables or t-SNE plots can make datasets difficult for non-bioinformaticians to interpret and compare. In order to remove these barriers and provide easy access to expression data for the proteins that regulate S-palmitoylation in the brain, we created 'BrainPalmSeq', an easy-to-use web platform allowing user-driven interrogation of compiled multi-study expression data at cellular resolution through simple interactive heatmaps that are populated according to user-selected brain regions, cell-types or genes of interest (<http://brainpalmseq.med.ubc.ca/>).

To create BrainPalmSeq we first curated three large datasets from whole-brain scRNAseq studies that were acquired through selection-free cell sampling to provide high-resolution expression data covering hundreds of cell types at a variety of developmental ages (Rosenberg et al., 2018; Saunders et al., 2018; Zeisel et al., 2018). As scRNAseq has several caveats including low sensitivity and high frequency of dropout events leading to incomplete detection of expressed genes (Haque et al., 2017), we complemented these datasets, where possible, with curation of several bulk and pooled-cell RNAseq studies that used population-level ensemble measurements from whole-brain and region-specific studies. We further included selected studies for the major glial cell types, and data from the most comprehensive neuron-specific study performed to date by the Allen Institute (Table 1). Together, the datasets curated in BrainPalmSeq cover all major regions of the mouse nervous system across a variety of regional and cellular resolutions.

Expression data were extracted from selected studies for the 24 mouse ZDHHC genes (*Zdhhc1*-*Zdhhc25*, while *Zdhhc10* is omitted), as well as the best characterized de-palmitoylating enzymes (*Ppt1*, *Lypla1*, *Lypla2*, *Abhd4*, *Abhd6*, *Abhd10*, *Abhd12*, *Abhd13*, *Abhd16a*, *Abhd17a*, *Abhd17b* and *Abhd17c*) and ZDHHC accessory proteins (*Golga7*, *Golga7b* and *Selenok*). Where possible, data were processed

from the raw transcripts or unique molecular identifier (UMI) counts using the same normalization protocol to allow for more consistent evaluation of differences in gene expression within datasets. We sampled from RNAseq datasets that used a diverse range of sample collection, processing and analysis techniques, allowing for direct visualization of the relative expression patterns of selected genes within datasets. Users can then validate their observations across complimentary whole-brain or region/cell-type specific datasets included in BrainPalmSeq. Dropdown menus allow for selection of individual ZDHHC genes or brain regions within each dataset, while the hover tool reveals metadata for each cell type, including neurotransmitter designations and marker genes. We provide download links to all expression data including cell type metadata so that users can replot gene expression profiles in their preferred format. To demonstrate the utility of this resource, we performed a detailed exploration of selected datasets from BrainPalmSeq, revealing how expression patterns can give insights into the function of the palmitoylating and de-palmitoylating enzymes in the mouse brain.

ZDHHC expression in the nervous system shows regional and cell-type specific patterning

We began by exploring BrainPalmSeq data curated from the ‘MouseBrain’ dataset, which provides the broadest overview of expression patterns in the nervous system (Zeisel et al., 2018). This scRNAseq study sampled multiple dissected regions from the adolescent (mean age ~P25) mouse central and peripheral nervous systems (CNS and PNS, respectively), identifying 265 transcriptomically unique cell-types (referred to herein as metacells) for which we plotted re-normalized ZDHHC expression values, according to the hierarchical cell-type clustering established by the original study (Figure 1A). While ZDHHC expression was detected in all regions of the nervous system, expression of the 24 ZDHHC genes was highly variable across metacell types and clusters. We measured the mean ZDHHC expression within each cluster to gain insight into which cell-types in the nervous system have the greatest overall expression of palmitoylating enzymes. The heatmap rows and columns were ranked (sorted by descending averages) to determine which cell-types had the highest expression of ZDHHCs, and which ZDHHCs were most abundantly expressed across cell-types (Figure 1B). Mean ZDHHC expression was particularly high in neurons of the PNS, along with cholinergic/monoaminergic and hindbrain neurons of the CNS. Of the non-neuronal metacell clusters, oligodendrocytes had the highest ZDHHC expression, while other glial cell-types appear at the lower end of the ranking (Figure 1B). *Zdhhc20* was the most abundantly expressed ZDHHC, with the highest mean expression across all cell-type clusters, followed by *Zdhhc2*, *Zdhhc17*, *Zdhhc3* and *Zdhhc21*, while expression of *Zdhhc11*, *Zdhhc19* and *Zdhhc25* were negligible. We next clustered neuronal metacells of the PNS and CNS according to the neurotransmitter expression combinations, revealing the highest mean ZDHHC expression was observed in neurons that

utilized acetylcholine and nitric oxide as co-neurotransmitters, with cholinergic neurons featuring near the top of the list in several neurotransmitter combinations (Figure 1C). Monoaminergic neurons utilizing noradrenaline and serotonin also generally ranked high in the list, consistent with the data in Figure 1B that ranked cholinergic and monoaminergic neurons as the metacell cluster with the highest CNS ZDHHC expression overall, indicating a higher propensity for these cell-types to utilize S-palmitoylation as a post-translational mechanism to modify cellular signaling. We performed comparative analysis of ZDHHC expression on another large-scale scRNAseq study of the mouse brain that sampled a variety of cortical and subcortical structures of the adult mouse (P60-P70) (Saunders et al., 2018; 'DropViz'; Figure 1-figure supplement 1A). We found expression patterns and enrichments to be similar across these two independent, large scale scRNAseq studies, supporting the general trends observed within the MouseBrain dataset.

To gain insight into the potential networks of ZDHHC enzymes that might work together to coordinate S-palmitoylation in different cell types we performed co-expression analysis (Spearman correlation) between ZDHHC genes across all 265 metacell types in the MouseBrain dataset (Figure 1D). Neuron-enriched *Zdhhc3*, *Zdhhc8*, *Zdhhc17* and *Zdhhc21* formed the strongest network of co-expression associations, while glial cell-enriched *Zdhhc2*, *Zdhhc9* and *Zdhhc20* formed less robust correlations with other ZDHHCs. Weaker correlations were observed across the 565 cell-types in the DropViz dataset, which may reflect the absence of the PNS neurons and glia in this study (Figure 1-figure supplement 1D). Interestingly, strong correlations were not observed for known pairs of palmitoylating enzymes that have been established to be functionally linked, including *Zdhhc20/Zdhhc5* (Plain et al., 2020) and *Zdhhc16/Zdhhc6* (Abrami et al., 2017). In the case of *Zdhhc20/Zdhhc5*, this could be due to the widespread expression of *Zdhhc20* throughout both neuronal and glial cell types in the nervous system, while *Zdhhc5* is predominantly expressed in neuronal cells. We plotted the expression values for each of the known pairs across 265 identified cell types from 'MouseBrain' dataset (Figure 4- figure supplement 2; data available for download on website). Co-expression was variable across cell types, indicating that the relationship between these pairs of enzymes may be cell-type specific.

In order to create a list of potential substrates for the ZDHHCs in the mouse nervous system, we expanded our co-expression analysis to include all expressed genes from the 'MouseBrain' dataset that had significant correlation ($R > 0.7$) with one or more ZDHHC. We identified 914 genes with expression patterns that were significantly correlated with ZDHHCs. This list was cross-referenced with the mouse SwissPalm database of S-palmitoylated substrates identified in at least one palmitoyl-proteome or

experimentally validated (SwissPalm annotated; Blanc et al., 2015, 2019). We found that genes that showed correlated expression with a ZDHHC were significantly enriched with S-palmitoylation substrates, indicating that ZDHHCs are more likely to be co-expressed with their S-palmitoylation substrates in the brain (Figure 1E). Co-expression analysis of the ‘DropViz’ dataset revealed a similar enrichment of S-palmitoylation substrates that were co-expressed with ZDHHCs (Figure 1-figure supplement 1E), supporting the notion of ZDHHC enzyme-substrate co-expression. PANTHER GO analysis of the ZDHHC co-expressed S-palmitoylation substrates curated from ‘MouseBrain’ revealed several significant enrichments in GO terms for biological processes related to protein localization and transport (Figure 1F). These findings are consistent with the known role of S-palmitoylation in regulating protein localization and signaling complexes at cellular membranes.

Heterogeneity in ZDHHC expression within excitatory neurons of the dorsal hippocampus

The hippocampus is a heavily studied brain region that is critical for learning and memory (Bird and Burgess, 2008). A recent pooled-cell RNAseq study of excitatory neurons in the hippocampus revealed extensive regional variability in gene expression profiles of the hippocampal tri-synaptic loop (hipposeq.janelia.org; Cembrowski et al., 2016). In order to clearly visualize if ZDHHC expression also varied within these different cell populations, we projected log transformed expression heatmaps generated in BrainPalmSeq for the ‘hipposeq’ dorsal-ventral excitatory neuron dataset on to anatomical maps of the dorsal hippocampus (Figure 2A). We observed considerable heterogeneity in the regional expression patterns of the ZDHHCs in the hippocampus. Hierarchical clustering analysis revealed that the ZDHHCs could be grouped into those that showed similar expression in all regions, those that were dentate gyrus granule cell (DG) enriched, DG depleted or CA1/CA2 enriched (Figure 2B). We generated comparative heatmaps for several scRNAseq studies curated in BrainPalmSeq that also quantified the hippocampal excitatory neuron transcriptome and found similar cross-study expression patterns for many of the ZDHHCs (Figure 2-figure supplement 1A). Furthermore, *in situ* hybridization data from the Allen Institute showed a high degree of overlap with the ‘hipposeq’ derived ZDHHC expression patterns, supporting the replicability of the expression patterns observed in the ‘hipposeq’ dataset (Figure 2-figure supplement 1B).

We next sought to utilize the ‘hipposeq’ dataset to determine if there might be regional differences in the expression of S-palmitoylation substrates in excitatory neurons of the dorsal hippocampus, which may be potential substrates for regionally enriched ZDHHC enzymes. We set out to create a ‘projected palmitoylome’ for neurons in each sub-region, consisting of genes that are both

enriched in each sub-region vs other sub-regions, and are also SwissPalm annotated. We utilized the enrichment analysis tools built in to hipposeq.janelia.org (see Materials and Methods). Neurons in each hippocampal sub-region expressed unique S-palmitoylation substrates that were related to highly divergent functions. We found for CA1 excitatory neurons, which have the highest expression of *Zdhhc2*, *Zdhhc17*, *Zdhhc23* and *Zdhhc9* (Figure 2C), the CA1 enriched projected palmitoylome (Figure 2D) generated KEGG pathways related to ‘Calcium signaling’, ‘Glutamatergic synapse’ and ‘Long term potentiation’, supporting the known role for S-palmitoylation in CA1 hippocampal synaptic plasticity (Figure 2E; Ji and Skup, 2021; Matt et al., 2019). The CA1 projected-palmitoylome was composed of around 46 % synaptic proteins (SynGO annotated), with SynGO ontologies related to ‘synaptic vesicle exocytosis’ and ‘synapse organization’ (Figure 2F; Koopmans et al., 2019). In contrast, the projected-palmitoylome of DG granule cells which have the highest expression of *Zdhhc21*, *Zdhhc4*, *Zdhhc24* and *Zdhhc8* (Figure 2G, H) generated KEGG pathways related to ‘Ribosome’, ‘Cholinergic synapse’ and ‘Parkinson’s disease’ (Figure 2I). The DG projected-palmitoylome was composed of 29 % synaptic proteins (SynGO annotated), with SynGO ontologies related to ‘protein translation at presynapse’ and ‘protein translation at postsynapse’, revealing a potential role for palmitoylating enzymes in regulating translation in this cell-type that has not yet been studied (Figure 2J). Together, we have described patterns of restricted expression of ZDHHC enzymes and S-palmitoylation substrates in the dorsal mouse hippocampus, and generated regionally-enriched projected-palmitoylomes that provide insight into the role of S-palmitoylation in neuronal function in each of these hippocampal sub-regions.

Neocortical ZDHHC expression is partially segregated across cortical layers and neuronal subclasses

We next examined scRNAseq datasets curated in BrainPalmSeq from the cortex, beginning with a study of the primary somatosensory cortex (SSp; Zeisel et al., 2015). We projected heatmaps of pyramidal excitatory neuron ZDHHC expression generated in BrainPalmSeq onto cortical layer diagrams of SSp, again revealing anatomically heterogeneous excitatory neuron expression patterns for several of the ZDHHC transcripts (Figure 3A). Clustering primarily grouped the enzymes according to expression levels, with *Zdhhc21*, *Zdhhc17* and *Zdhhc8* displaying the highest relative expression (Figure 3B). *Zdhhc2*, *Zdhhc3* and *Zdhhc20* expression was also high, with the remainder of the ZDHHCs having moderate to low expression. We compared these expression patterns with other datasets curated in BrainPalmSeq (Figure 3-figure supplement 1A), which revealed many consistent patterns of expression maintained across several independent studies. For example, multiple studies reported high expression of *Zdhhc8* in cortical Layer 2/3, enrichment of *Zdhhc2* in Layer 4 and elevated expression of *Zdhhc21* in all layers, particularly in Layer 5. *Zdhhc3* and *Zdhhc20* were also broadly expressed in all cortical layers across

studies. Similar patterns were seen in the SSp region from available in situ hybridization studies from Allen Brain Institute (Figure 3-figure supplement 1B).

We examined expression patterns of the ZDHHC enzymes from one of the largest neuronal scRNAseq studies from the isocortex performed by the Allen Brain Institute, which identified 236 glutamatergic and 117 GABAergic distinct neuron metacell types (Yao et al., 2021). We averaged ZDHHC expression data downloaded from BrainPalmSeq for the major metacell clusters from all regions of the isocortex, according to their anatomical location and/or axon projection and plotted ranked heatmaps (Figure 3C,D). *Zdhhc14* was the ZDHHC transcript with the highest expression across glutamatergic neurons, while *Zdhhc2* was one of the highest expressed enzymes in the majority of GABAergic cell-types. Elevated expression of *Zdhhc14* was found in both glutamatergic and GABAergic neurons, which was moderately expressed in other studies of the brain and cortex discussed previously. Glutamatergic neurons in cortical layers 4/5, 5 and 6 featured at the top of the ranking for highest overall expression of ZDHHC enzymes. Neurons within these layers have extensive dendritic branching and long-range axonal projections to the spinal cord, brainstem and midbrain, as well as the ipsilateral cortex, striatum and thalamus (Harris and Shepherd, 2015; Yao et al., 2021). GABAergic neurons of the isocortex also showed elevated expression of the common neuronal ZDHHCs including *Zdhhc2*, *Zdhhc3*, *Zdhhc17*, *Zdhhc20* and *Zdhhc21*. The highest mean ranked expression was observed in the recently categorized Sncg neurons that correspond to Vip⁺/Cck⁺ multipolar or basket cells (Tasic et al., 2018), and lowest expression was observed in the Vip subclass of interneurons.

Together, our observations reveal that the complex transcriptional diversity of neurons that has recently been revealed by RNA sequencing also includes heterogeneity in the expression of the ZDHHC enzymes that mediate palmitoylation. These expression patterns are likely to influence enzyme-substrate interactions along with the function of S-palmitoylation substrates, and thus influence neuronal development, function and synaptic plasticity.

De-palmitoylating enzyme and ZDHHC accessory protein expression in the nervous system shows regional and cell-type specific patterning

Dynamic turnover of protein S-palmitoylation is mediated by the activity of de-palmitoylating enzymes, which determine the half-life of S-palmitoylation on a target protein. Among the first of these enzymes to be discovered were acyl-protein thioesterases 1 and 2 (APT1, APT2; encoded by *Lypla1*, *Lypla2*) and palmitoyl-protein thioesterase 1 (PPT1), which are all members of the serine hydrolase family. However, full characterization of this family of proteins is ongoing, with over 100 members of the

serine hydrolase superfamily being identified to date (Simon and Cravatt, 2010). Not all of these proteins have been found to exhibit depalmitoylating activity, therefore we limited our study to include those that are blocked by palmitoylation inhibitors that mimic the palmitoyl acyl chain, including Palmostatin B and hexadecylfluorophosphonate (Lin et al., 2017). These included a number of the α/β hydrolase domain-containing proteins (ABHD4, ABHD6, ABHD10, ABHD12, ABHD13, ABHD16A, ABHD17A, ABHD17B and ABHD17C). Compared with the ZDHHC enzymes, relatively less is known about the substrates, sub-cellular localization and brain expression patterns of this family of enzymes. We next explored BrainPalmSeq to determine which cell-types/brain regions show the highest expression of de-palmitoylating enzymes.

We first examined expression heatmaps for the known de-palmitoylating enzymes across the 265 cell-types identified in the 'MouseBrain' dataset (Figure 4A) and the cell-type averages for the 565 cell-types from the 'DropViz' dataset (Figure 4-figure supplement 1A). *Abhd12*, which is a membrane-bound enzyme that also has an important role in lysophosphatidylserine metabolism, and is associated with neurodegenerative disorder PHARC (polyneuropathy, hearing loss, ataxia, retinosis pigmentosa, and cataract; Blankman et al., 2013), had the broadest expression across all cell-types. This was followed by *Ppt1*, with expression of both of these enzymes being notably elevated in neurons of the hindbrain and immune cells. *Abhd4* was highly enriched in glial cells, particularly astrocytes, with low expression across neuronal subtypes in both datasets, consistent with previous reports of colocalization of *Abhd4* mRNA with astrocyte marker, *Slc1a3* (László et al., 2020). Ranked expression (sorted by descending averages) of de-palmitoylating enzymes in the 'MouseBrain' (Figure 4B) and 'DropViz' (Figure 4-figure supplement 1B) revealed that *Abhd12*, *Abhd17a*, *Ppt1*, *Abhd17b* and *Abhd16a* were the highest expressed depalmitoylating enzymes across studies. *Lypla2* expression was greater than *Lypla1* overall in the brain, with *Lypla2* expression being highest in neurons and ependymal cells (Figure 4-figure supplement 1A). *Abhd17c* had the lowest brain expression of all the de-palmitoylating enzymes studied. Correlation analysis between the ZDHHCs and de-palmitoylating enzymes revealed numerous instances of co-expression with almost every ZDHHC (Figure 4D), revealing potential cooperative pairs of palmitoylating and de-palmitoylating enzymes in the nervous system.

Although the ZDHHC enzymes are thought to act autonomously, several accessory proteins have been discovered that can regulate ZDHHC stability, localization and catalytic activity (Salaun et al., 2020). These include GOLGA7 (GCP16), which can bind to ZDHHC9 and enhance both protein stability and enzymatic activity by stabilizing the ZDHHC9 auto-palmitoylated intermediate that is formed prior to

palmitate transfer from the enzyme to the substrate protein (Mitchell et al., 2014; Swarthout et al., 2005). Both GOLGA7 and related isoform GOLGA7B are also able to interact with ZDHHC5, with the latter influencing ZDHHC5 plasma membrane localization (Woodley and Collins, 2019). Finally, SELENOK (SELK; Selenoprotein K) is an ER localized protein that was found to interact with ZDHHC6, stabilize the auto-palmitoylated intermediate and increase palmitoylation of substrate proteins including the IP₃ receptor (Fredericks et al., 2017, 2014). We observed widespread expression of *Selenok* across all cell-types, with expression being considerably higher than any of the ZDHHCs, de-palmitoylating enzymes or other accessory proteins (Figure 4A, Figure 4-figure supplement 1A). This is consistent with the known functions of SELENOK in the ER-associated protein degradation pathway and regulation of ER calcium flux (Pitts and Hoffmann, 2018). *Golga7b* expression was widespread across neuronal subtypes but barely detected in glial cells (Figure 4A, S4A). Accordingly, *Golga7b* expression was also strongly correlated with several of the ZDHHCs that were most highly expressed in neurons, including *Zdhhc3*, *Zdhhc8*, *Zdhhc17* and *Zdhhc21* (Figure 4D). In contrast, *Golga7* was enriched in glial cells, particularly in oligodendrocytes, similar to ZDHHC9 for which GOLGA7 is a key accessory protein (Figure 4A, Figure 4-figure supplement 1A). Overall, the co-expression between putative *Zdhhc*/accessory protein pairs detailed above (*Zdhhc5/Golga7b*; *Zdhhc9/Golga7*; *Zdhhc6/Selenok*) was relatively weak (Figure 4E), therefore we plotted the expression values for each of the known pairs across 265 identified cell types from 'MouseBrain' dataset (Figure 4-figure supplement 2). We found that while *Zdhhc5* is expressed in several cell types with little-to-no expression of *Golga7b*, *Zdhhc9* and *Zdhhc6* were not expressed in the absence of their accessory proteins (*Golga7* and *Selenok*, respectively) in any cell type. Co-expression of *Zdhhc5/Golga7b* was highest in neuronal subtypes (Figure 4-figure supplement 2A), while *Zdhhc9/Golga7* co-expression was highest in oligodendrocytes, indicating there may be certain cellular contexts in which these pairings might be particularly important.

Cell type enrichment of mRNA is partially maintained at the protein level

Previous studies have reported that mRNA and protein quantities can be poorly correlated due to post-transcriptional processing. These changes in protein degradation or synthesis can alter steady-state protein abundance (Vogel and Marcotte, 2012). We next set out to determine the extent to which the cell-type RNA expression patterns of the palmitoylation associated genes are maintained at the protein level, utilizing data from an available proteomic study of pooled isolated cells (MACS microbead plus antibody isolation) from neonatal mouse brains (Sharma et al., 2015), which we compared the protein abundance with scRNAseq expression from similarly aged neonatal mice (Rosenberg et al., 2018). Focusing on proteins from our list of genes that were detected in all four cell types in the

proteomic dataset, we calculated cell type z-scores for mRNA or protein abundance in each study and compared enrichment patterns (Figure 4-figure supplement 3; Figure 4 – Source data 4). While we found numerous instances of similar patterns of cell-type enrichment for both mRNA and protein, including proteins that were primarily enriched in astrocytes (Figure 4-figure supplement 3B), microglia (Figure 4-figure supplement 3C), neurons (Figure 4-figure supplement 3D) and oligodendrocytes (Figure 4-figure supplement 3E), we also observed instances where this was not the case (Figure 4-figure supplement 3F). Notably, several highly expressed genes from the RNAseq study were not detected at the protein level in any cell type, including ZDHHC2, ZDHHC9 and SELENOK, which may be due to poor depth of coverage in the proteomic screen, or may indicate that these genes may be subject to more extensive post-transcriptional regulation. Overall, we found a significant correlation ($r = 0.63$, $p < 0.0001$) when plotting mRNA vs protein z-score across all cell types for the identified genes (Figure 4 - Figure supplement 3G). Together, these results indicate that the cell-type mRNA enrichment for many of the family of proteins that mediate S-palmitoylation is maintained at the protein level. Future advances in single-cell proteomics, along with tandem studies of both RNA and protein in the brain, will enable more precise comparison between the cell-type transcriptome and proteome.

Loss of function mutations in palmitoylating and de-palmitoylating enzymes

Impaired regulation of S-palmitoylation has been implicated in numerous neurological disorders, many of which are due to loss of function (LOF) mutations in the genes encoding palmitoylating and de-palmitoylating enzymes (Cho and Park, 2016; Matt et al., 2019). We next sought to determine if the regional and cell-type expression data available in BrainPalmSeq could reveal insights into the pathogenesis of disorders caused by LOF mutations in palmitoylating and de-palmitoylating enzymes. As many of these diseases have a neurodevelopmental origin, we examined whole brain datasets curated in BrainPalmSeq from the neonatal (Rosenberg et al., 2018), adolescent (Zeisel et al., 2018) and adult (Sjöstedt et al., 2020) mouse brain.

A single nucleotide polymorphism (SNP) in the *ZDHHC8* gene has been implicated in increased susceptibility to schizophrenia (Chen et al., 2004; Mukai et al., 2004), while hemizygous microdeletion in the chromosomal locus 22q11, which encodes a number of genes including *ZDHHC8*, is one of the highest known genetic risk factors to developing schizophrenia (Figure 5A; Karayiorgou et al., 2010). To assess the developmental expression of *Zdhhc8*, we averaged expression within broadly defined cell-type clusters that could be applied to both the Rosenberg and Zeisel scRNAseq datasets (Figure 5A, B; Supplementary File 1). *Zdhhc8* expression was highest in neurons of the cortex and hippocampus,

followed by neurons of the mid- and hindbrain at both developmental ages. To explore regional expression in the adult mouse brain, we projected BrainPalmSeq generated heatmaps expression data from the 'Protein Atlas' mouse whole brain dataset (bulk RNAseq from major brain regions; Figure 5-figure supplement 1) onto anatomical maps of the mouse brain, again revealing highest expression of *Zdhhc8* in the cortex, followed by the hippocampus and basal ganglia (Figure 5C; Sjöstedt et al., 2020). *Zdhhc8* expression was particularly enriched in Layer 2/3 of the neonatal (not shown) and adult mouse (Figure S3B) cortex, which is the cortical layer with the most pronounced morphological deficits in patients with Schizophrenia (Glantz and Lewis, 2000; Kolluri et al., 2005; Wagstyl et al., 2016). Together, we found *Zdhhc8* expression patterns in the mouse brain that are established early in postnatal development and maintained into adulthood, that also overlay with many brain regions and cell types that are known to be severely affected in patients with schizophrenia. These observations support a model in which LOF *ZDHHC8* mutations may elicit many of the symptoms of schizophrenia by disrupting S-palmitoylation and normal neuronal development in these brain regions.

Mutations in the *ZDHHC9* gene, which is located on the X chromosome, have been identified in ~2% of individuals with X-linked intellectual disability (ID) (Raymond et al., 2007; Tzschach et al., 2015). Neuroanatomical abnormalities reported in patients with *ZDHHC9* mutations include decreased cortical, thalamic and striatal volume, as well as widespread white matter abnormalities with prominent hypoplasia (under-development) of the corpus callosum (Baker et al., 2015; Bathelt et al., 2016). Disrupted white matter integrity is thought to underlie deficits in global and local brain connectivity in patients with *ZDHHC9* mutations (Bathelt et al., 2017). *Zdhhc9* knock-out mice also develop similar pathological changes, including decreased volume of the corpus callosum (Kouskou et al., 2018). We observed considerable cell-type enrichment of *Zdhhc9* in oligodendrocytes across studies and developmental ages (Figure 5D, E), accompanied by moderate neuronal expression of *Zdhhc9* relative to other *ZDHHCs* across several brain regions including the hippocampus and cortex (Figure 2A, 3A, 5D, E), consistent with the known function of *ZDHHC9* in regulating neuronal development (Shimell et al., 2019). Regionally, we found *Zdhhc9* expression in adult mice to be highly enriched in the corpus callosum, the largest white matter tract in the brain (Figure 5F). As myelin production by oligodendrocytes is critical for maintaining white matter integrity, these observations indicate that disrupting S-palmitoylation in oligodendrocytes may underlie the white matter pathology and decreased connectivity observed in patients with X-linked ID and *ZDHHC9* mutations.

Infantile neuronal ceroid lipofuscinosis (INCL or CLN1 disease) is a severe neurological disorder caused by LOF mutations in the *PPT1* gene that presents in the first 6 - 12 months of life and is characterized by rapid developmental regression, blindness and seizures, with continual deterioration until death in early childhood (Nita et al., 2016). While PPT1 is thought to primarily localize to lysosomes with an essential role in lysosomal degradation of S-palmitoylated proteins (Lu et al., 1996), this protein also has a synapse-specific function in regulating synaptic vesicle cycling and synaptic transmission (Koster et al., 2021; Koster and Yoshii, 2019). We found that neuronal *Ppt1* expression was high in postnatal neurons of the spinal cord, olfactory bulb and mid/hindbrain, while microglia were the highest expressing non-neuronal cell type at both postnatal ages (Figure 5G, H). Neurodegeneration has been detected in the spinal cord prior to onset within the brain in *Ppt1* knock-out mice, accompanied by extensive glial cell activation including microgliosis, which is a pathological hallmark of CLN1 disease (Shyng et al., 2017). Mid-/hindbrain neurons also had high expression of *Ppt1*, consistent with reports that *Ppt1* knock-out mice show early signs of brain pathology in the thalamus (Kielar et al., 2007). Overall, we observed widespread *Ppt1* expression in almost every brain region in adult mice, consistent with the sweeping neurological deficits associated with CLN1 disease (Figure 5I). Together, these observations reveal how the loss of *Ppt1* in cell types with high *Ppt1* expression may lead to cell death/dysfunction in the early stages of CLN1 disease.

ZDHHC cell type enrichments can be used to predict and validate ZDHHC substrates

We next tested if ZDHHC expression patterns identified from BrainPalmSeq could be used to predict and validate S-palmitoylation substrates for regionally enriched ZDHHCs. We focused on *Zdhhc9*, which showed a consistent cell-type enrichment in oligodendrocytes across multiple studies in BrainPalmSeq, while LOF mutations in *ZDHHC9* are known to result in reduced white matter integrity in the brain (Raymond et al., 2007). Examination of the Marques et al oligodendrocyte-specific scRNAseq dataset curated in BrainPalmSeq revealed that oligodendrocyte *Zdhhc9* expression increased throughout maturation, with highest expression in the myelin forming (MFOL) intermediate-maturity subtype of oligodendrocytes, while slightly lower expression is maintained in mature oligodendrocytes (MOL; Figure 6A; Marques et al., 2016).

To identify potential substrates for ZDHHC9, we cross-referenced a list of MFOL/MOL enriched genes identified in the study by Marques et al (Marques et al., 2016) with the SwissPalm database to identify known palmitoylation substrates in these cell types (Swiss Palm Annotated; Figure 6B; Blanc et al., 2019, 2015). PANTHER analysis of cellular component enrichments for these substrates revealed the

most significant enrichment was for the term ‘myelin sheath’ (30 proteins; Figure 6C, Figure 6-figure supplement 1). To determine if any of the myelin sheath associated proteins could be palmitoylated by ZDHHC9, we selected three proteins (MOBP, PLP1 and CNP) for experimental validation (Figure 6C). We separately expressed each of these candidate substrates together with ZDHHC9 and its accessory protein GOLGA7 in HEK293T cells, and determined the proportion of palmitoylated substrate using an acyl-resin assisted capture (acyl-RAC) palmitoylation assay (Forrester et al., 2011). Co-expression of HA-ZDHHC9 and FLAG-GOLGA7 increased the palmitoylated fraction of MOBP and PLP1, indicating that these proteins are substrates for ZDHHC9 (Figure 6D, E, G). Conversely, CNP was not identified as a ZDHHC9 substrate in our assay (Figure 6F, G). While ZDHHC9 is able to palmitoylate MOBP and PLP1 in HEK cells, we observed no change in the palmitoylation of these substrates in *Zdhhc9* knock-out mice (P23 half brain) compared to wild-type (Figure 6 – Figure supplement 2). It is possible that ZDHHC9 is not required for the palmitoylation of these proteins *in vivo* (i.e. compensation by other ZDHHC enzymes), or that the detection of differences in protein palmitoylation requires isolation of specific cell populations that can be diluted using whole-brain lysate as has been previously reported (Gorenberg et al., 2022; Kouskou et al., 2018). Overall, these results demonstrate how the cell-type enrichments of ZDHHC enzymes identified in this study can be used, along with the lists of similarly enriched palmitoylation substrates, to guide the identification of enzyme-substrate interactions that can be further investigated *in vivo*.

Discussion

BrainPalmSeq as a tool to generate hypotheses about proteins that control S-palmitoylation in the brain

We have demonstrated the utility of BrainPalmSeq by providing examples of how this database can be used to explore detailed region and cell type-specific expression patterns of the known palmitoylating and de-palmitoylating enzymes, and their accessory proteins. We reveal how these expression patterns can be used to predict/validate S-palmitoylation substrates and better understand diseases associated with loss of function mutations in the enzymes that mediate S-palmitoylation. Given the number of brain regions and cell types incorporated into BrainPalmSeq that were not discussed in the present study, including the thalamus, hypothalamus, amygdala, striatum and cerebellum, there is rich potential for users to explore the data and generate hypotheses about the role of these enzymes in the brain.

Insights into the role of S-palmitoylation associated enzymes in brain physiology and pathology

While we found that many of the proteins we studied showed correlated expression across the entire mouse nervous system, particularly those enriched in neurons including *Zdhhc3*, *Zdhhc8*, *Zdhhc17* and *Zdhhc21*, expression of these genes was segregated within more narrowly defined neuronal populations such as the excitatory pyramidal neurons within the hippocampal tri-synaptic loop or layers of the somatosensory cortex. This is in line with the extensive neuronal transcriptional heterogeneity identified recently by a number of scRNAseq studies (Saunders et al., 2018; Yao et al., 2021; Zeisel et al., 2018, 2015). The genes that determine neuronal identity fall under four broad functional categories: those that control transcriptional programs, membrane conductance, neurotransmission, or synaptic connectivity (Zeisel et al., 2018). We also report heterogeneity in the neuronal fingerprint of palmitoylating and de-palmitoylating enzyme expression, which will in turn give rise to differential S-palmitoylation of neuronal proteins. Future work is needed to determine how these specific ZDHHC expression patterns are related to dynamic S-palmitoylation in these neuronal sub-types, and how the elevated expression of certain ZDHHCs can alter neuronal function. Given that S-palmitoylation is a key regulator of neuronal development, and that nearly half of all known synaptic proteins are substrates for palmitoylation (Sanders et al., 2015), this heterogeneity is likely to be a key mechanism in the fine tuning of neuronal function and synaptic transmission.

Many of the ZDHHCs that we observed with consistently elevated expression across multiple studies in BrainPalmSeq have already been studied in the context of neuronal signaling, including ZDHHC2, ZDHHC3, ZDHHC8 and ZDHHC17 (Ji and Skup, 2021; Matt et al., 2019). In contrast, ZDHHC20 and ZDHHC21 are relatively understudied in the nervous system, despite our observation that these are two of the most abundantly expressed ZDHHCs across neuronal cell types, with broad expression of *Zdhhc20* also in glial cells. A recent study defined a role for ZDHHC21 in the palmitoylation of serotonergic receptor 5-HT1A and implicated downregulation of ZDHHC21 in the development of major depressive disorder (Gorinski et al., 2019). Interestingly, both ZDHHC20 and ZDHHC21 have a potential role in the pathogenesis of Alzheimer's disease, as they can palmitoylate BACE1, Tau and amyloid precursor protein (Cho and Park, 2016). Further work is required to understand the likely important role of these enzymes in the brain.

We made several other interesting observations during our examination of BrainPalmSeq that were not discussed in detail in the present study but we believe warrant further investigation. For example, the particularly elevated expression of *Zdhhc2* in peripheral sensory neurons may indicate an

important role for palmitoylation in this cell type. Across multiple studies we observed striking enrichment of *Zdhhc14* in cerebellar Purkinje neurons, a cell type in which S-palmitoylation is known to be important for long-term depression, although the role of ZDHHC14 in this process has not yet been investigated (Thomas et al., 2013). *Zdhhc23* was similarly enriched in the CA2 region of the hippocampus, with comparatively low expression across other cell types. More broadly, the elevated expression of a variety of palmitoylating enzymes in neurons that utilize acetylcholine or monoamines as neurotransmitters would suggest an important role for S-palmitoylation in these neurons that has yet to be explored. Accordingly, many of the key proteins involved in cholinergic synaptic transmission are S-palmitoylation substrates including muscarinic acetylcholine receptor M2 (CHRM2), acetylcholinesterase (ACHE) and ATP-citrate synthase (ACLY; Blanc et al., 2015, 2019). Our observations of co-enrichment of certain palmitoylating and de-palmitoylating enzymes are also of interest, such as *Abhd17b* and *Zdhhc9* in oligodendrocytes. It is possible that these enzymes share substrates to mediate dynamic palmitoylation/de-palmitoylation, or conversely, have separate substrates in order to maintain stable S-palmitoylation states of certain oligodendrocyte expressed proteins. Importantly, the data accessibility in BrainPalmSeq will enable researchers to develop hypotheses regarding their cell type, brain region or protein of interest.

The palmitoylome of each cell type in the nervous system is likely to be highly heterogeneous and will be determined by the expression of both the S-palmitoylation substrates and the palmitoylating and de-palmitoylating enzymes in a given cell type. Furthermore, accumulating evidence has revealed that this palmitoylome can be altered by extrinsic factors such as chronic stress and neuronal activity (Kang et al., 2008; Zareba-Kozioł et al., 2019). While we have provided projected palmitoylomes composed of several highly expressed or enriched S-palmitoylation substrates in select brain regions and cell types, experimental validation to reveal the relative palmitoylation of substrates under various conditions is needed to fully understand these cellular differences. Nevertheless, we were able to utilize our projected palmitoylomes to validate substrates for ZDHHC9, providing insight into the potential role of this enzyme in myelin regulation in the brain.

Neurological disorders that arise from LOF gene mutations may be predicted to lead to pathological changes that are more severe in the brain regions in which these genes are most highly expressed. We observed this type of regional overlap for the expression patterns of *Zdhhc8*, *Zdhhc9* and *Ppt1*. Numerous other brain disorders are thought to be exacerbated by an imbalance in S-palmitoylation, such as decreased S-palmitoylation of HTT in Huntington's disease (Virlogeux et al.,

2021; Yanai et al., 2006), increased S-palmitoylation of APP and TAU in Alzheimer's disease (Cho and Park, 2016), and reduced S-palmitoylation of 5-HTA receptor in major depressive disorder (Gorinski et al., 2019). Efforts are already underway to normalize aberrant S-palmitoylation in neurological diseases in order to improve clinical outcomes (Roberts et al., 2012; Virlogeux et al., 2021). Understanding the brain expression patterns of the enzymes that mediate palmitoylation in these diseases will be paramount to developing and targeting such therapeutics.

While scRNAseq has proven to be a groundbreaking tool that has helped identify many unique cell types in the brain while allowing a means to study cellular gene expression patterns at remarkable depth, characterization of the proteome of individual brain cells has lagged behind transcriptome profiling. This is largely due to the inability to amplify protein in the same way as RNA, greatly reducing the depth of coverage observed compared with transcriptomic analyses. Instead, proteomic studies generally utilize pooled cell isolation methods to improve detection (Goto-Silva and Junqueira, 2021; Wilson and Nairn, 2018). Proteomic analysis is particularly important as previous studies have found that RNA and protein abundance are often moderately correlated, as a result of post-translational processing of protein or RNA molecules. Our comparison of mRNA and protein abundance in the major brain cell types during postnatal development revealed numerous instances of similar cell-type enrichments for the majority of the proteins detected. This would imply that while the absolute amount of mRNA and protein may differ in a given cell type, the mRNA cell-type enrichments are predictive of protein enrichment for many of the genes included in our study.

Differential gene expression as a means to control S-palmitoylation in the brain

The mechanisms that govern ZDHHC enzyme-substrate interactions are complex and still not fully understood. While the majority of post-translational modifications including phosphorylation and N-glycosylation are highly sequence specific (Schwarz and Aebi, 2011; Ubersax and Ferrell, 2007), several studies have revealed that S-palmitoylation by ZDHHCs can be stochastic, proximity based and lacking in stereo-selectivity (Rocks et al., 2010; Rodenburg et al., 2017). Contrasting studies have shown that numerous ZDHHCs have specific protein interacting domains including ankyrin repeat (AR), PDZ and SH3 domains that facilitate substrate interactions, providing support for a model in which more specific enzyme-substrate interactions can govern S-palmitoylation (Abrami et al., 2017; Lemonidis et al., 2015; Plain et al., 2020; Rana et al., 2018; Thomas et al., 2012; Verardi et al., 2017). Furthermore, a recent study found striking substrate specificity for several ZDHHCs with the G-protein subunit Gαo, and revealed intriguing observations that the subcellular localization of a number of S-palmitoylation

substrates could be controlled by changing the localization, and importantly, the expression of certain ZDHHC enzymes. In this study, S-palmitoylated substrates were found to accumulate in the subcellular compartment in which their partner ZDHHCs were targeted (Solis et al., 2022). This is particularly relevant as the ZDHHCs are known to have diverse subcellular localizations including the Golgi, ER, endosomes and plasma membrane (Globa and Bamji, 2017). Transcriptional control of differentially compartmentalized palmitoylating and de-palmitoylating enzymes could therefore be an essential mechanism for regulating the subcellular localization, and function, of S-palmitoylated protein substrates. Accordingly, LOF mutations in certain ZDHHC enzymes leads to cell type-specific disruption in S-palmitoylation that is not compensated by other members of the large ZDHHC family. We provide a means to investigate the expression of the proteins that regulate S-palmitoylation, making BrainPalmSeq an invaluable resource to both researchers and clinicians that are working to better understand the role of S-palmitoylation in the brain.

570 **List of Abbreviations**
571 ABHD: α/β hydrolase domain-containing
572 APT: acyl-protein thioesterase
573 CA1: Cornu Ammonis-1
574 CA2: Cornu Ammonis-2
575 CA3: Cornu Ammonis-3
576 CNS: Central nervous system
577 COP: Comitted oligodendrocyte precursor
578 CT: Corticothalamic
579 DG: Dentate gyrus
580 GABA: γ -Aminobutyric acid
581 GC: Granule cell
582 Glu: Glutamate
583 HC: Hippocampus
584 HPF: Hippocampal formation
585 IT: Intratelencephalic
586 MFOL: Myelin forming oligodendrocyte
587 MOL: Mature oligodendrocyte
588 NFOL: Newly formed oligodendrocyte
589 NP: Near projecting
590 OPC: Oligodendrocyte precursor cell
591 PNS: Peripheral nervous system
592 PPT: palmitoyl-protein thioesterases
593 PT: Pyramidal tract
594 scRNAseq: single-cell RNA sequencing
595 SP: SwissPalm
596 SSp: Primary somatosensory cortex

597

598

First Author	Year	PMID	Regions	Age	Website	Technique	Sample	Data Accession
Zeisel	2018	30096314	CNS/PNS	Juvenile	http://mousebrain.org/	10X Genomics	Single-cell	
Saunders	2018	30096299	Whole brain	Adult (P60-70)	http://dropviz.org/	Drop-seq	Single-cell	GSE116470
Sjöstedt	2020	32139519	Whole brain	Adult	https://www.proteinatlas.org/	RNA-seq	Bulk tissue	
Rosenberg	2018	29545511	Whole brain	Neonatal	n/a	SPLiT-seq	Single-cell	GSE110823
Cembrowski	2016	27113915	Hippocampus	Adult	http://hipposeq.janelia.org/	Genetic labeling; RNA-seq	Cell sorted	GSE74985
Zhang	2014	25186741	Cortex	Adult	http://web.stanford.edu/group/barr-es_lab/brain_rnaseq . https	PAN; FACS; RNA-seq	Cell sorted	GSE52564
Zeisel	2015	25700174	Cortex, hippocampus CA1	Adult	http://linnarssonlab.org/cortex	Fluidigm C1	Single-cell	GSE60361
Yao	2021	34004146	Isocortex/ hippocampus	Adult (P50+)	https://celltypes.brain-map.org/rnaseq/mouse_ctx-hip_10x	10X Genomics	Single-cell	
Kozareva	2020	24259518	Cerebellum	Adult	https://singlecell.broadinstitute.org/single_cell/study/SCP795	snSeq; 10x Chromium V3	Single-cell	
Phillips	2019	31527803	Thalamic excitatory neurons	Adult	https://thalamoseq.janelia.org/	NextSeq 550	Single-cell/bulk tissue	GSE133911; GSE133912
Chen	2017	28355573	Hypothalamus	Adult	n/a	Drop-seq	Single-cell	GSE87544
Gocke	2016	27425622	Striatum	Adult	n/a	Smart-seq2	Single-cell	GSE82187
O'Leary	2020	32869744	Amygdala excitatory neurons	Adult	https://scrnaseq.janelia.org/amygdala	scRNAseq	Single-cell	GSE148866
Marques	2016	27284195	Oligodendrocytes whole brain	Juvenile; adult	http://linnarssonlab.org/oligodendrocytes/	Fluidigm C1	Single-cell	GSE75330
Batiuk	2020	32139688	Astrocytes in cortex/ hippocampus	Adult (P56+)	https://holt-sc.glialab.org/sc/	Smart-seq2	Single-cell	GSE114000
Li	2019	30606613	Microglia in brain	Embryonic, juvenile, adult	https://www.brainrnaseq.org/	Smart-seq2	Single-cell	GSE123025

599 **Table 1. RNAseq published datasets curated to create BrainPalmSeq**

Figure Legends

Figure 1. Heterogeneous ZDHHC expression in the mouse nervous system

(A) Heatmap showing expression for the 24 ZDHHC genes, extracted from scRNAseq study of mouse CNS and PNS (Zeisel et al., 2018). Each column represents one of the 265 metacells classified in the study. Metacells are organized along x-axis according to hierarchical clustering designations generated by Zeisel et al. Full metadata for this study available on BrainPalmSeq.

(B) Heatmap showing mean ZDHHC expression per hierarchical cluster, with columns and rows sorted by descending mean ZDHHC expression per row/column.

(C) Heatmap showing mean ZDHHC expression per neurotransmitter cluster for all PNS and CNS neurons. Columns and rows are sorted as in B.

(D) Correlation network showing ZDHHC co-expression across all metacells in 'MouseBrain' (Spearman $R > 0.5$). Numbers in nodes correspond to ZDHHC number. Node color represents mean expression across all metacells. Edge thickness represents strength of correlation.

(E) Graph showing proportion of genes from 'MouseBrain' dataset that are co-expressed with one or more ZDHHC and also substrates for S-palmitoylation (SwissPalm annotated). 'Brain expressed' $n = 15,389$ protein coding genes expressed in the postnatal mouse brain, curated from the MGI RNAseq studies database. ' $R > 0.7$ ZDHHC co-expressed' $n = 914$ genes co-expressed with one or more ZDHHC (Spearman $R > 0.7$). ' $R > 0.8$ ZDHHC co-expressed' $n = 167$ genes co-expressed with one or more ZDHHC (Spearman $R > 0.8$). Brain expressed vs. $R > 0.7$: $p < 0.001$; $R > 0.7$ vs $R > 0.8$: $p < 0.01$; Fisher's exact test.

(F) Graph of GO biological process analysis. Gene IDs from the 'MouseBrain' dataset (Zeisel et al., 2018) that showed correlated expression with one or more ZDHHC ($R > 0.7$) and were also Uniprot reviewed and SwissPalm annotated were used as input.

Units for all heatmaps in figure: mean $\log_2(\text{counts per } 10,000 + 1)$.

Figure 2. Diversity in ZDHHC expression and S-palmitoylation substrate expression in the hippocampus

(A) Heatmap of excitatory neuron ZDHHC expression from dorsal hippocampus (original pooled cell RNAseq data from Cembrowski et al., 2016) projected onto diagrams of dorsal hippocampus.

(B) Hierarchical clustering of ZDHHC expression data in A.

(C) Heatmap showing top 6 ranked expressing ZDHHCs in dorsal CA1 in descending order.

(D) Pie chart showing proportion genes with enriched expression in dorsal CA1 (dCA1) that are also substrates for palmitoylation (SwissPalm annotated).

(E) KEGG analysis of the dCA1 enriched/SwissPalm annotated genes.

(F) SynGO analysis of the dCA1 enriched/SwissPalm annotated genes.

(G-J) As in (C)-(F) but for the dorsal dentate gyrus (dDG).

Heatmap legend in (A) applies to all heatmaps ($\log\text{FPKM}+1$).

Figure 3. Pyramidal neuron layer specific ZDHHC expression

(A) Heatmap of excitatory neuron ZDHHC expression from somatosensory cortex (original data scRNAseq data from Zeisel et al., 2015) projected onto diagrams of cortical layers.

(B) Hierarchical clustering of ZDHHC expression data in A. Heatmap units in (A, B): mean $\log_2(\text{counts per } 10,000 + 1)$

(C) Heatmap of scRNAseq data from Allen Brain 10X genomics (Yao et al., 2021). Data are represented as mean ZDHHC expression per excitatory neuron subtype, with columns and rows sorted by descending mean ZDHHC expression per row/column.

(D) As in (C) but for inhibitory neuron subtypes. Heatmap units for (C, D): trimmed mean (25%-75%) $\log_2(\text{CPM}+1)$

Figure 4. Heterogeneous de-palmitoylating enzyme and ZDHHC accessory protein expression in the mouse nervous system

(A) Heatmap showing expression of de-palmitoylating enzymes (top) and ZDHHC accessory subunits (bottom), extracted from scRNAseq study of mouse CNS and PNS (Zeisel et al., 2018). Each column represents one of the 265 metacells classified in the study. Metacells are organized according to hierarchical clustering designations generated by Zeisel et al.

(B) Heatmap showing mean de-palmitoylating enzyme expression per hierarchical cluster, with columns and rows sorted by descending mean ZDHHC expression per row/column.

(C) As B but for ZDHHC accessory proteins.

(D) Correlation network showing ZDHHC co-expression with de-palmitoylating enzymes and accessory proteins across all metacells in 'MouseBrain' (Spearman $R > 0.4$). Node color represents mean expression across all metacells. Edge thickness represents strength of correlation.

Figure 5. Disease associated palmitoylating enzyme regional and cell-type expression overlays with brain pathology in associated LOF disorders

(A) Heatmap showing ranked *Zdhhc8* expressing neuronal and glial cell types in descending order. Original data from scRNAseq neonatal mouse brain study; Rosenberg et al., 2018. Cell types were averaged as described in Supplementary File 1. Heatmap units: mean $\log_2(\text{counts per } 10,000 + 1)$.

(B) As in A, but original data from scRNAseq adolescent mouse brain study Zeisel et al (2018). Heatmap units: mean $\log_2(\text{counts per } 10,000 + 1)$.

(C) Heatmap of *Zdhhc8* expression from whole brain regional bulk RNAseq data (original data from 'Protein Atlas'; Sjöstedt et al., 2020) projected onto anatomical map of mouse brain. Heatmap units: pTPM.

(D-F) As in (A)-(C) but for *Zdhhc9*.

(G-I) As in (A)-(C) but for *Ppt1*.

Figure 6. Validation of projected S-palmitoylation substrates of *Zdhhc9* derived from cell-type enriched expression

(A) Graph of expression data for *Zdhhc9* extracted from BrainPalmSeq. Original data from oligodendrocyte scRNAseq study by Marques et al. Expression units: mean log2(counts per 10,000 + 1).

(B) Diagram illustrating workflow to generate a list of oligodendrocyte enriched palmitoylation substrates, GO annotated for myelin sheath for experimental validation.

(C) STRING diagram of myelin sheath annotated palmitoylation substrates.

(D) Western blot following Acyl-RAC palmitoylation assay in HEK293 cells to identify palmitoylated and unpalmitoylated fractions of FLAG-MOBP either without or with co-transfection of FLAG-GOLGA7 and HA-ZDHHC9. Input = unprocessed protein lysate. NSB control = non-specific binding of protein to sepharose resin in control pipeline. Palm fraction = palmitoylated protein. Unpalm fraction = unpalmitoylated protein.

(E-F) As in (D) but for FLAG-PLP1 (E) or FLAG-CNP (F).

(G) Graphs quantifying the ratio of palmitoylated to unpalmitoylated protein either with or without co-transfections with FLAG-GOLGA7 and HA-ZDHHC9. $n = 4-6$ HEK cell cultures per condition. Statistics shown for palmitoylated fraction. Two-way ANOVA; Šidák's *post hoc*; mean \pm SEM. MOBP: $p = 0.0004$, 95% CI -0.6594 to -0.2266; PLP1: $p = 0.0046$, 95% CI -0.1660 to -0.03011; CNP: $p = 0.6981$, 95% CI -0.3274 to 0.1742.

Supplementary Figure Legends

Figure 1 - Figure supplement 1. Heterogeneous ZDHHC expression in the mouse brain

(A) Heatmap showing expression for the 24 ZDHHC genes, extracted from 'DropViz' scRNAseq study of mouse brain (Saunders et al., 2018). Each column represents metacell averages. Metacells are organized along x-axis according to brain region (neuronal) or class (non-neuronal). Full metadata for this study available on BrainPalmSeq.

(B) Heatmap showing mean *Zdhhc* expression per brain region/class, with columns and rows sorted by descending mean *Zdhhc* expression per row/column.

(C) Heatmap showing mean *Zdhhc* expression per neurotransmitter cluster for neurons from all brain regions. Columns and rows are sorted as in B.

(D) Correlation network showing ZDHHC co-expression across all metacells in 'DropViz' (Spearman $R > 0.5$). Numbers in nodes correspond to ZDHHC number. Node color represents mean expression across all metacells. Edge thickness represents strength of correlation.

(E) Graph showing proportion of genes from 'DropViz' dataset that are co-expressed with one or more ZDHHC and also substrates for S-palmitoylation (SwissPalm annotated). 'Brain expressed' = 15,389 protein coding genes expressed in the postnatal mouse brain, curated from the MGI RNAseq studies database. ' $R > 0.7$ ZDHHC co-expressed' = 676 genes co-expressed with one or more ZDHHC (Spearman $R > 0.7$).

704 Units for all heatmaps in figure: mean log2(counts per 10,000 + 1).

705 **Figure 1- Figure supplement 2. Correlation of Zdhhc enzymes that are known to be involved in**
706 **palmitoylation cascades.**

707 (A) Plot of Zdhhc5 vs Zdhhc20 expression across 265 identified cell types from 'MouseBrain' dataset.
708 Expression units: mean log2(counts per 10,000 + 1). Arrows/labels indicate 'MouseBrain' cell types that
709 have high expression of both genes. Legend below indicates annotation of these cell types.

710 (B) As (A), but for Zdhhc6 vs Zdhhc16.

711 **Figure 2 - Figure supplement 1. Heterogeneous ZDHHC expression in excitatory neurons of the**
712 **hippocampus**

713 (A) Heatmaps showing ZDHHC expression data from BrainPalmSeq for excitatory neurons of indicated
714 subregions of the hippocampus. Original data are from 'Hipposeq' (Cembrowski et al., 2016; units:
715 FPKM), 'DropViz' (Saunders et al., 2018; units: mean log2(counts per 10,000 + 1)) and Allen Mouse Brain
716 10X atlas (Yao et al., 2021; units: Trimmed Mean (25%-75%) Log2(CPM+1)).

717 (B) Expression maps from Figure 2A with in-situ hybridization images from Allen Brain ISH.

718 **Figure 3-figure supplement 1. Heterogeneous ZDHHC expression in excitatory neurons of the cortex**

719 (A) Heatmaps showing ZDHHC expression data from BrainPalmSeq for excitatory neurons of indicated
720 layers of the cortex. Original data are from somatosensory cortex (Zeisel et al., 2015; units: mean
721 log2(counts per 10,000 + 1)); 'MouseBrain' (Zeisel et al., 2018; mean log2(counts per 10,000 + 1);
722 'DropViz' posterior cortex (Saunders et al., 2018; units: mean log2(counts per 10,000 + 1)) and Allen
723 Mouse Brain 10X atlas intertelencephalic neurons (Yao et al., 2021; units: Trimmed Mean (25%-75%)
724 Log2(CPM+1)).

725 (B) Expression maps from Figure 3A with in-situ hybridization images of somatosensory cortex from
726 Allen Brain ISH.

727 **Figure 4 - figure supplement 1. Heterogeneous de-palmitoylating enzyme and accessory protein**
728 **expression in mouse brain**

729 (A) Heatmap showing expression for the 6 depalmitoylating enzyme genes and 3 accessory protein
730 genes extracted from 'DropViz' scRNAseq study of mouse brain (Saunders et al., 2018). Each column
731 represents metacell averages. Metacells are organized along x-axis according to brain region (neuronal)
732 or class (non-neuronal). Full metadata for this study available on BrainPalmSeq. Expression units: mean
733 log2(counts per 10,000 + 1).

734 (B) Heatmap showing mean expression of the 6 depalmitoylating enzyme genes per brain region/class,
735 with columns and rows sorted by descending mean gene expression per row/column.

736 (C) Heatmap showing mean expression of the 3 accessory protein genes per brain region/class, with
737 columns and rows sorted by descending mean gene expression per row/column.

738 **Figure 4-figure supplement 2. Correlation of Zdhhc enzymes and their known accessory proteins**

739 (A) Plot of *Zdhhc5* vs *Golga7b* expression across 265 identified cell types from 'MouseBrain' dataset.
740 Expression units: mean log2(counts per 10,000 + 1). Arrows/labels indicate 'MouseBrain' cell types that
741 have high expression of both genes. Legend below indicates annotation of these cell types.

742 (B) As (A), but for *Zdhhc9* vs *Golga7*.

743 (C) As (A), but for *Zdhhc6* vs *Selenok*.

744 **Figure 4-figure supplement 3. Cell-type enrichment of ZDHHC and depalmitoylating enzyme protein**

745 (A) Bioinformatic workflow to calculate mRNA and protein z-scores in each major brain cell type.

746 (B) Heatmaps showing genes with mRNA and protein predominantly enriched in astrocytes.

747 (C-F) As (B), but for microglia, neurons, oligodendrocytes and inconsistently enriched cells.

748 (G) Graph showing correlation of protein vs RNA z-scores for all genes in each of the cell types
749 investigated.

750 **Figure 5-figure supplement 1. Anatomical sampling for bulk RNAseq study**

751 (A) Diagram illustrating anatomical brain regions for bulk RNA expression data from Figure 5 (Sjöstedt et
752 al., 2020).

753 **Figure 6-figure supplement 1. GO cellular component analysis for oligodendrocyte enriched genes**

754 (A) Graph of GO cellular component analysis. Gene IDs from the full Marques oligodendrocyte dataset
755 (Marques et al., 2016) that were enriched in MFOL and MOL subtypes and were also Uniprot reviewed
756 and SwissPalm annotated were used as input.

757 **Figure 6-figure supplement 2. Palmitoylation of myelin proteins in *Zdhhc9* KO mice**

758 (A) Western blot following Acyl-RAC palmitoylation assay in WT or *Zdhhc9* KO half-brains to identify
759 palmitoylated and unpalmitoylated fractions of CNP, PLP1 and MOBP. Input = unprocessed protein
760 lysate. Palm fraction = palmitoylated protein. Unpalm fraction. = unpalmitoylated protein.

761 (B) Graphs quantifying the ratio of palmitoylated to unpalmitoylated protein in WT or *Zdhhc9* KO mice. *n*
762 = 2-3 animals per condition. Statistics shown for palmitoylated fraction. Two-way ANOVA; Šídák's *post*
763 *hoc*; mean ± SEM. ns = not significant.

764 **Source Data Legends**

765 **Figure 1 – Source data 1.** ZDHHC expression in the mouse nervous system from 'MouseBrain' dataset
766 (related to Figure 1A)

767 **Figure 1 – Source data 2.** Depalmitoylating enzyme and *Zdhhc* accessory protein expression (cell type
768 averages) from 'MouseBrain' dataset (related to Figure 4B,C)

769 **Figure 1 Source data 3.** ZDHHC neurotransmitter averages from 'MouseBrain' dataset (related to Figure
770 1C)

771 **Figure 1 Source data 4:** Spearman correlations 'MouseBrain' dataset (related to Figure 1D)

772 **Figure 1 Source data 5:** Spearman correlations of S-palmitoylation associated genes vs all other genes in
773 'MouseBrain' dataset ($R > 0.7$) (related to Figure 1E)

774 **Figure 1 Source data 6:** Panther analysis of palmitoylation substrates (SwissPalm annotated) co-
775 expressed with any Zdhhc ($R > 0.7$) (related to Figure 1F)

776 **Figure 1-figure supplement 1-source data 1.** Mean cell type ZDHHC expression in the mouse brain
777 system from 'DropViz' dataset (related to Figure 1 – figure supplement 1A).

778 **Figure 1-figure supplement 1-source data 2.** DropViz Zdhhc expression averaged by neurotransmitter
779 (related to Figure 1 – figure supplement 1C).

780 **Figure 1-figure supplement 1-source data 3.** Spearman correlation between Zdhhc genes across 565 cell
781 types in 'DropViz' dataset (related to Figure 1 – figure supplement 1D)

782 **Figure 1-figure supplement 1-source data 4.** Spearman correlations of S-palmitoylation associated
783 genes vs all other genes in 'DropViz' dataset ($R > 0.7$) (related to Figure 1 - figure supplement 1E)

784

785 **Figure 2 – Source data 1.** Neuronal expression of Zdhhc genes in dorsal hippocampus from 'HippoSeq'
786 dataset (related to Figure 2A, B, C, G).

787 **Figure 2 – Source data 2.** Dorsal CA1 (dCA1) enriched projected palmitoylome (related to Figure 2D, E,
788 F).

789 **Figure 2 – Source data 3.** KEGG Analysis of regionally enriched neuron expressed palmitoylation
790 substrates (related to Figure 2E, I).

791 **Figure 2 – Source data 4.** SynGO Analysis of regionally enriched neuron expressed palmitoylation
792 substrates (related to Figure 2F, J).

793 **Figure 2 – Source data 5.** Dorsal Dentate Gyrus (dDG) enriched projected palmitoylome (related to
794 Figure 2D, E, F).

795 **Figure 2 - figure supplement 1-source data 1.** Expression of Zdhhcs in hippocampal excitatory neurons
796 across RNAseq studies (related to Figure 2 – figure supplement 1A).

797 **Figure 2 - figure supplement 1-source data 2.** In situ hybridization images used from Allan Brain Atlas
798 (related to Figure 2 – figure supplement 1B).

799

800 **Figure 3 – Source data 1.** Zdhhc expression cortical layers from 'Zeisel et al 2015' (Related to figure 3A,
801 B).

802 **Figure 3 – Source data 2.** Zdhhc expression by excitatory neuron (subtype mean) from Allen Brain 10X
803 mouse dataset (Related to figure 3C).

804 **Figure 3 – Source data3.** Zdhhc expression by inhibitory neuron (subtype mean) from Allen Brain 10X
805 mouse dataset (Related to figure 3D).

806 **Figure 3 - figure supplement 1 - source data 1.** Expression of Zdhhcs in cortical excitatory neurons
807 across RNAseq studies (related to Figure 3 – figure supplement 1A).

808 **Figure 3 - figure supplement 1-source data 2.** In situ hybridization images used from Allan Brain Atlas
809 (related to Figure 3 – figure supplement 1B).

810

811 **Figure 4 – Source data 1.** Depalmitoylating enzyme and Zdhhc accessory protein expression in the
812 mouse nervous system from 'MouseBrain' dataset (related to Figure 4A).

813 **Figure 4 – Source data 2.** Depalmitoylating enzyme and Zdhhc accessory protein expression (cell type
814 averages) from 'MouseBrain' dataset (related to Figure 4B, C).

815 **Figure 4 – Source data 3.** Spearman correlations of all palmitoylation associated genes from
816 'MouseBrain' dataset (related to Figure 4D,E).

817 **Figure 4 - figure supplement 1 - source data 1.** De-palmitoylating enzyme and Zdhhc accessory
818 expression (cell type mean) DropViz (related to Figure 4 – figure supplement 1).

819 **Figure 4 - figure supplement 3 - source data 1.** Calculation of cell type z-scores from Rosenberg et al
820 2018 RNAseq and Sharma et al 2015 proteomics (related to figure 4-figure supplement 3).

821 **Figure 5 – Source data 1.** Disease associated palmitoylating enzyme regional and cell-type expression
822 patterns (related to Figure 5).

823 **Figure 6 – Source data 1.** Zdhhc9 expression in oligodendrocytes, Marques et al., 2016.

824 **Figure 6 – Source data 2.** S-palmitoylation substrates enriched in myelinating and mature
825 oligodendrocytes (related to Figure 6B, C).

826 **Figure 6 – Source data 3.** Acyl Rac quantification for Zdhhc9 substrate validation (related to Figure

827 **Figure 6 – Source data 4-31.** Uncropped raw and annotated Western blot images for all data quantified
828 in figure 6G.

829

830 **Materials and Methods**831 **Key Resources Table**

Key Resources Table				
Reagent type (species) or resource	Designation	Source or reference	Identifiers	Additional information
Recombinant DNA reagent	FLAG-GOLGA7	Gift from Maurine Linder Washington University School of Medicine		
Recombinant DNA reagent	HA-DHHC9	Shimell et al., 2019		
Recombinant DNA reagent	FLAG-MOBP	Origene, Maryland, USA	CAT#: RC223946	
Recombinant DNA reagent	FLAG-PLP1	Origene, Maryland, USA	CAT#: RC218616	
Recombinant DNA reagent	FLAG-CNP	Origene, Maryland, USA	CAT#: RC207038	
cell line (<i>Homo-sapiens</i>)	HEK293T	ATCC	CAT # CRL-1573	
antibody	anti-HA, (rabbit monoclonal)	Cell Signaling Technology	CAT#: 3724	Dilution 1:1000

antibody	anti-FLAG (mouse monoclonal)	Origene	CAT#: TA50011-100	Dilution 1:000
antibody	anti-MOBP (Rabbit polyclonal)	Invitrogen	CAT# PA5-100618	1:1000
antibody	anti-PLP1 (Rabbit polyclonal)	abcam	CAT# ab28486	1:1000
antibody	anti-CNP (Mouse monoclonal)	abcam	CAT# ab6319	1:1000
commercial assay or kit	CAPTUREome S- palmitoylated protein kit	Badrilla, UK	CAT# K010-311	

832

833 **Data processing for BrainPalmSeq**

834 For Zeisel et al., 2018 ('MouseBrain'), single-cell counts (UMI from 3' end counting) were downloaded
835 from MouseBrain.org (loom file named I5_all.loom), and log normalized by first scaling the expression
836 values provided to a sum of 10,000 per cell before calculating $\log_2(\text{scaled_counts}+1)$. Averages were
837 then performed by brain region, neurotransmitter and taxonomy for each gene.

838 For DropViz Metacell counts were downloaded from DropViz.org (count file
839 metacells.BrainCellAtlas_Saunders_version_2018.04.01.RDS and annotation file
840 annotation.BrainCellAtlas_Saunders_version_2018.04.01.RDS) and log normalized by first scaling the
841 expression values provided to a sum of 10,000 per metacell before calculating $\log_2(\text{scaled_counts}+1)$.
842 Averages were then performed by cell type, tissue and class for each gene. Genes associated with
843 palmitoylation were selected in order to create the heatmaps.

844 For Zeisel, single-cell counts (UMI from 3' end counting) were downloaded from
845 [https://storage.googleapis.com/linnarsson-lab-www-blobs/blobs/cortex/expression_mRNA_17-Aug-](https://storage.googleapis.com/linnarsson-lab-www-blobs/blobs/cortex/expression_mRNA_17-Aug-2014.txt)
846 2014.txt, and log normalized by first scaling the expression values provided to a sum of 10,000 per cell
847 before calculating $\log_2(\text{scaled_counts}+1)$. Averages were then performed by cluster, tissue and class for
848 each gene. Genes associated with palmitoylation were selected in order to create the heatmaps,
849 categories comprising fewer than 5 single cells are not displayed.

850 For Marques, single-cell counts (UMI from 3' end counting) were downloaded from GEO with accession
851 ID GSE75330 (file GSE75330_Marques_et_al_mol_counts2.tab) and log normalized by first scaling the
852 expression values provided to a sum of 10,000 per cell before calculating $\log_2(\text{scaled_counts}+1)$.
853 Averages were then performed by cluster and region for each gene. Genes associated with
854 palmitoylation were selected in order to create the heatmaps, categories comprising fewer than 5 single
855 cells are not displayed.

856 For Rosenberg, single-cell counts (UMI from 3' end counting) were downloaded from GSE110823, and
857 log normalized by first scaling the expression values provided to a sum of 10,000 per cell before
858 calculating $\log_2(\text{scaled_counts}+1)$. Averages were then performed by brain region, neurotransmitter and
859 taxonomy for each gene. Genes associated with palmitoylation were selected in order to create the
860 heatmaps.

861 Data from Sjöstedt et al. were downloaded as Protein-coding transcripts per million (pTPM) from
862 proteinatlas.org ("RNA mouse brain region gene data") and not further processed.

863 For Hipposeq, expression data were downloaded as FKPM directly from hipposeq.janelia.org and were
864 not further processed.

865 For Allen Brain 10X data, expression data were downloaded as trimmed means (25%-75%) $\log_2(\text{CPM}+1)$
866 from portal.brain-map.org/ and were not further processed.

867 **Correlation analysis**

868 Spearman correlation values between genes and their significances were calculated in R using the
869 expression results obtained for each cell type as described above.

870 **Identification of S-palmitoylation substrates with SwissPalm**

871 Gene lists were inputted into SwissPalm (<https://swisspalm.org/proteins>) input file function and cross-
872 referenced with 'Dataset 3: Palmitoylation validated or found in at least one palmitoyl-proteome
873 (SwissPalm annotated)' for *Mus musculus*, with an additional filter for UniProt 'Reviewed' proteins.

874 **Generating a projected palmitoylome for dorsal hippocampus**

875 To curate the regionally enriched projected-palmitoylome, the enrichment analysis tools in hipposeq
876 (<https://hipposeq.janelia.org/>) were used to compare each of the selected Cell Lines vs the other Cell
877 Lines in the analysis (Selected Cell Lines = dorsal DG, CA3, CA2 and CA1), with the following parameters:
878 'Fold threshold' = 1.5; 'FKPMmin threshold' = 5, 'FDR' = 0.05. The resulting lists of regionally enriched
879 transcripts were cross referenced with SwissPalm as described above to identify regionally enriched S-
880 palmitoylation substrates.

881 **Bioinformatic analysis**

882 Gene Ontology (GO) analysis was performed using statistical overrepresentation tests in PANTHER16.0
883 (Mi et al., 2009) with default settings and *Mus musculus* as the reference species. Biological process GO
884 terms were extracted and ranked according to false discovery rate (FDR). Kyoto Encyclopedia of Genes
885 and Genomes (KEGG) analysis was performed using the web-based program Enrichr (Chen et al., 2013;
886 Kuleshov et al., 2016) and ranked according to $-\log$ Adjusted P-value. Synaptic Gene Ontologies (SynGO;
887 version 1.1) analysis was performed using default settings with brain expressed genes as a background

and terms for ‘biological process’ were ranked according to -log Adjusted P-value. Functional protein interaction networks were identified using the Search Tool for the Retrieval of Interacting Genes (STRING) 11.0 (Szklarczyk et al., 2019) with *Mus musculus* as the reference species. Seven types of protein interactions were used for network generation, including text mining, neighborhood, co-occurrence, co-expression, gene fusion, experiments and databases.

Data presentation

Heatmaps were plotted and hierarchical clustering performed in Displayr (<https://www.displayr.com>) using the ‘Dendrogram’ function. Cytoscape (Version 3.8.0) was used to draw correlation networks.

Heatmap creation for BrainPalmSeq

All plots for the BrainPalmSeq database were generated using curated RNA sequencing datasets. Python 3 and Javascript scripts were used with the plotting library Bokeh to generate the interactive heatmaps to display and compare these datasets on the BrainPalmSeq website (Bokeh Development Team, 2018).

Cell culture

HEK293T cells were purchased from ATCC (CRL-1573) and the cell line was authenticated by STR profiling and confirmed negative for mycoplasma. Cells were thawed and aliquoted into a 10cm dish with 10mL prewarmed (37°C) DMEM (GIBCO, Thermo Fisher Scientific, Waltham, MA) supplemented with 10% fetal bovine serum (FBS) (GIBCO, Thermo Fisher Scientific, Waltham, MA) and 1% Pen/Strep(P/S) (GIBCO, Thermo Fisher Scientific, Waltham, MA). HEK293T cells were then placed in a 37°C incubator with 5% CO₂ and passaged approximately every 5 days, or once confluency was achieved.

Transfection

70%-80% confluent HEK293T cells were transfected using Lipofectamine 2000 (Invitrogen/Life Technologies, Carlsbad, CA) according to the manufacturer’s recommendations. Each well of a 6-well plate was transfected with a total of 3ug DNA, 150uL of Opti-Mem (GIBCO, Thermo Fisher Scientific, Waltham, MA) was used with 6uL of Lipofectamine 2000 (Invitrogen/Life Technologies, Carlsbad, CA). Experimental condition wells were transfected with 1ug of the indicated construct of interest, 1ug of HA-DHHC9 (mouse; Shimell et al., 2019), and 1ug of FLAG-GOLGA7 (Maurine Linder, Washington University School of Medicine). Human FLAG-MOBP (CAT#: RC223946), FLAG-PLP1 (CAT#: RC218616) and FLAG-CNP (CAT#: RC207038) were acquired from Origene, Maryland, USA. Control condition wells were transfected with 1ug of the indicated construct of interest, and 2ug of a scrambled control plasmid. Cells were lysed using the acyl-RAC assay lysis buffer 48hours after transfection.

Palmitoylation Assay (acyl-RAC)

The commercially available CAPTUREome S-palmitoylated protein kit (Badrilla, Leeds, UK) was used in accordance with the manufacturer’s guidelines with three optimizations: (1) prior to the cell lysis step, wells were washed with 1mL of 1X PBS to eliminate any dead cells or residual media; (2) during the cell lysis step, DNase (Sigma-Aldrich, St. Louis, MO), was added to the solution (5uL per 500uL of lysis buffer); and (2) protein concentration was measured prior to the separation of experimental sample and negative control sample using the BCA Assay (Pierce, Thermo Fisher Scientific, Waltham, MA).

Western Blot Analysis

Western blotting was performed using 4% stacking and 12% resolving SDS-PAGE gels. PVDF membranes were then blocked for 1 hour at room temperature with 5% BSA in 0.05% TBS-T. PVDF membranes were incubated with the indicated primary antibodies (anti-HA: Cell Signaling Technology, C29F4, Rabbit mAb CAT#: 3724, 1:1000; anti-FLAG: Origene, mouse monoclonal antibody, CAT#: TA50011-100, 1:1000) overnight at 4°C. Proteins were then visualized using enhanced chemiluminescence (Immubilon Western Chemiluminescent HRP Substrate) on a BioRad ChemiDoc XRS+ scanner. Blots were then quantified using Fiji1 software. The palmitoylated and unpalmitoylated fractions were calculated using the following equations respectively: $100 \times (\text{Palm Fraction} - \text{NSB} / ((\text{Palm Fraction} - \text{NSB}) + \text{Unpalm Fraction}))$ and $100 \times (\text{Unpalm Fraction} / (\text{Palm Fraction} + \text{Unpalm Fraction}))$. Criteria for data inclusion were sufficient transfection/antibody signal and minimal protein in the non-specific binding control.

Animals

All experimental procedures and housing conditions were approved by the UBC Animal Care Committee and were in accordance with the Canadian Council on Animal Care (CCAC) guidelines. Male C57BL/6J mice (Jackson Laboratory, Sacramento, CA) were bred with female heterozygous *Zdhhc9* knockout mice (B6;129S5-Zdhhc9tm1Lex/Mmucd) obtained from the Mutant Mouse Resource and Research Center (MMRRC) at the University of California, Davis. Mice were bred and genotyped as described in (Shimell et al., 2019). For acyl-RAC assays, litter matched knockout and wild-type males were used at P22-P24.

Preparation of brain lysate

Brains were removed and immediately flash frozen in isopentane (-55 °C). Half brains (not including cerebellum) were lysed in the acyl-RAC kit blocking buffer first using a pestle and then passing through a 26-gauge needle. The samples were then processed following the acyl-RAC protocol as described above.

Statistical Analysis

Spearman correlations were performed with the function `cor` in R, and their significances were obtained using the function `cor.test` followed by a correction for multiple testing using `p.adjust` with the `fdr` method (Benjamini & Hochberg). For assessing enrichment of S-palmitoylation substrates within *Zdhhc* co-expressed genes, Fisher's exact test was performed using the function `fisher.test` in R.

For validation of substrates using Acyl-Rac palmitoylation assay, two-way ANOVA with Šídák's *post hoc* was used to assess significance of both palmitoylated and unpalmitoylated fractions. Statistics are shown for palmitoylated fraction. No outliers were excluded. Statistical analyses were performed in GraphPad Prism 9.2.0 (San Diego, CA, USA). *n* represents the number of individual HEK cell culture dishes. Each culture dish is defined as a biological replicate. No technical replicates were performed.

Acknowledgements

The authors would like to thank Drs. A. Ciernia, M. Cembrowski, T. Murphy and J. LeDue for helpful discussion.

Funding Information

This work was supported by CIHR Foundation grant (F18-00650) to SXB and by computational resources made available through the NeuroImaging and NeuroComputation Centre at the Djavad Mowafaghian

964 Centre for Brain Health (RRID SCR_019086) and the Dynamic Brain Circuits in Health and Disease
965 Research Excellence Cluster DataBinge Forum.

References

- Abrami L, Dallavilla T, Sandoz PA, Demir M, Kunz B, Savoglidis G, Hatzimanikatis V, van Der Goot FG. 2017. Identification and dynamics of the human ZDHC16-ZDHC6 palmitoylation cascade. *eLife* **6**. doi:10.7554/eLife.27826
- Baker K, Astle DE, Scerif G, Barnes J, Smith J, Moffat G, Gillard J, Baldeweg T, Raymond FL. 2015. Epilepsy, cognitive deficits and neuroanatomy in males with ZDHC9 mutations. *Annals of Clinical and Translational Neurology* **2**:559–569. doi:10.1002/acn3.196
- Bathelt J, Astle D, Barnes J, Raymond FL, Baker K. 2016. Structural brain abnormalities in a single gene disorder associated with epilepsy, language impairment and intellectual disability. *NeuroImage: Clinical* **12**:655–665. doi:10.1016/j.nicl.2016.07.016
- Bathelt J, Barnes J, Raymond FL, Baker K, Astle D. 2017. Global and Local Connectivity Differences Converge With Gene Expression in a Neurodevelopmental Disorder of Known Genetic Origin. *Cerebral Cortex* **27**:3806–3817. doi:10.1093/cercor/bhx027
- Bird CM, Burgess N. 2008. The hippocampus and memory: Insights from spatial processing. *Nature Reviews Neuroscience* **9**:182–194. doi:10.1038/nrn2335
- Blanc M, David F, Abrami L, Migliozi D, Armand F, Bürgi J, van der Goot FG. 2015. SwissPalm: Protein Palmitoylation database. *F1000Research* **4**. doi:10.12688/f1000research.6464.1
- Blanc M, David FPA, van der Goot FG. 2019. SwissPalm 2: Protein S-palmitoylation database Methods in Molecular Biology. Humana Press Inc. pp. 203–214. doi:10.1007/978-1-4939-9532-5_16
- Blankman JL, Long JZ, Trauger SA, Siuzdak G, Cravatt BF. 2013. ABHD12 controls brain lysophosphatidylserine pathways that are deregulated in a murine model of the neurodegenerative disease PHARC. *Proceedings of the National Academy of Sciences of the United States of America* **110**:1500–1505. doi:10.1073/pnas.1217121110
- Chen EY, Tan CM, Kou Y, Duan Q, Wang Z, Meirelles G V., Clark NR, Ma'ayan A. 2013. Enrichr: Interactive and collaborative HTML5 gene list enrichment analysis tool. *BMC Bioinformatics* **14**. doi:10.1186/1471-2105-14-128
- Chen WY, Shi YY, Zheng YL, Zhao XZ, Zhang GJ, Chen SQ, Yang P Di, He L. 2004. Case-control study and transmission disequilibrium test provide consistent evidence for association between schizophrenia and genetic variation in the 22q11 gene ZDHC8. *Human Molecular Genetics*

995 **13**:2991–2995. doi:10.1093/hmg/ddh322

996 Cho E, Park M. 2016. Palmitoylation in Alzheimer’s disease and other neurodegenerative diseases.
997 *Pharmacological Research* **111**:133–151. doi:10.1016/j.phrs.2016.06.008

998 Forrester MT, Hess DT, Thompson JW, Hultman R, Moseley MA, Stamler JS, Casey PJ. 2011. Site-specific
999 analysis of protein S-acylation by resin-assisted capture. *Journal of Lipid Research* **52**:393–398.
1000 doi:10.1194/JLR.D011106/ATTACHMENT/AA2B322B-A63D-41C0-A864-92DAC7C09076/MMC1.PDF

1001 Fredericks G, Hoffmann F, Hondal R, Rozovsky S, Urschitz J, Hoffmann P. 2017. Selenoprotein K Increases
1002 Efficiency of DHHC6 Catalyzed Protein Palmitoylation by Stabilizing the Acyl-DHHC6 Intermediate.
1003 *Antioxidants* **7**:4. doi:10.3390/antiox7010004

1004 Fredericks GJ, Hoffmann FKW, Rose AH, Osterheld HJ, Hess FM, Mercier F, Hoffmann PR. 2014. Stable
1005 expression and function of the inositol 1,4,5-triphosphate receptor requires palmitoylation by a
1006 DHHC6/selenoprotein K complex. *Proceedings of the National Academy of Sciences of the United*
1007 *States of America* **111**:16478–16483. doi:10.1073/pnas.1417176111

1008 Fukata Y, Dimitrov A, Boncompain G, Vielemeyer O, Perez F, Fukata M. 2013. Local palmitoylation cycles
1009 define activity-regulated postsynaptic subdomains. *Journal of Cell Biology* **202**:145–161.
1010 doi:10.1083/jcb.201302071

1011 Fukata Y, Fukata M. 2010. Protein palmitoylation in neuronal development and synaptic plasticity.
1012 *Nature Reviews Neuroscience*. doi:10.1038/nrn2788

1013 Glantz LA, Lewis DA. 2000. Decreased dendritic spine density on prefrontal cortical pyramidal neurons in
1014 schizophrenia. *Archives of General Psychiatry* **57**:65–73. doi:10.1001/archpsyc.57.1.65

1015 Globa AK, Bamji SX. 2017. Protein palmitoylation in the development and plasticity of neuronal
1016 connections. *Current Opinion in Neurobiology*. doi:10.1016/j.conb.2017.02.016

1017 Gorenberg EL, Tieze SM, Yücel B, Zhao HR, Chou V, Wirak GS, Tomita S, Lam TKT, Chandra SS. 2022.
1018 Identification of substrates of palmitoyl protein thioesterase 1 highlights roles of depalmitoylation
1019 in disulfide bond formation and synaptic function. *PLoS Biology* **20**:e3001590.
1020 doi:10.1371/journal.pbio.3001590

1021 Gorinski N, Bijata M, Prasad S, Wirth A, Abdel Galil D, Zeug A, Bazovkina D, Kondaurova E, Kulikova E,
1022 Ilchibaeva T, Zareba-Kozioł M, Papaleo F, Scheggia D, Kochlamazashvili G, Dityatev A, Smyth I,

1023 Krzystyniak A, Wlodarczyk J, Richter DW, Strekalova T, Sigrist S, Bang C, Hobuß L, Fiedler J, Thum T,
1024 Naumenko VS, Pandey G, Ponimaskin E. 2019. Attenuated palmitoylation of serotonin receptor 5-
1025 HT1A affects receptor function and contributes to depression-like behaviors. *Nature*
1026 *Communications* **10**:1–14. doi:10.1038/s41467-019-11876-5

1027 Goto-Silva L, Junqueira M. 2021. Single-cell proteomics: A treasure trove in neurobiology. *Biochimica et*
1028 *Biophysica Acta - Proteins and Proteomics*. doi:10.1016/j.bbapap.2021.140658

1029 Haque A, Engel J, Teichmann SA, Lönnberg T. 2017. A practical guide to single-cell RNA-sequencing for
1030 biomedical research and clinical applications. *Genome Medicine* **9**:1–12. doi:10.1186/s13073-017-
1031 0467-4

1032 Harris KD, Shepherd GMG. 2015. The neocortical circuit: Themes and variations. *Nature Neuroscience*
1033 **18**:170–181. doi:10.1038/nn.3917

1034 Ji B, Skup M. 2021. Roles of palmitoylation in structural long-term synaptic plasticity. *Molecular Brain*
1035 **14**:1–27. doi:10.1186/s13041-020-00717-y

1036 Kang R, Wan J, Arstikaitis P, Takahashi H, Huang K, Bailey AO, Thompson JX, Roth AF, Drisdell RC, Mastro
1037 R, Green WN, Yates JR, Davis NG, El-Husseini A. 2008. Neural palmitoyl-proteomics reveals dynamic
1038 synaptic palmitoylation. *Nature* **456**:904–909. doi:10.1038/nature07605

1039 Karayiorgou M, Simon TJ, Gogos JA. 2010. 22q11.2 microdeletions: Linking DNA structural variation to
1040 brain dysfunction and schizophrenia. *Nature Reviews Neuroscience* **11**:402–416.
1041 doi:10.1038/nrn2841

1042 Kolluri N, Sun Z, Sampson AR, Lewis DA. 2005. Lamina-specific reductions in dendritic spine density in
1043 the prefrontal cortex of subjects with schizophrenia. *American Journal of Psychiatry* **162**:1200–
1044 1202. doi:10.1176/appi.ajp.162.6.1200

1045 Koopmans F, van Nierop P, Andres-Alonso M, Byrnes A, Cijssouw T, Coba MP, Cornelisse LN, Farrell RJ,
1046 Goldschmidt HL, Howrigan DP, Hussain NK, Imig C, de Jong APH, Jung H, Kohansalnodehi M,
1047 Kramarz B, Lipstein N, Lovering RC, MacGillavry H, Mariano V, Mi H, Ninov M, Osumi-Sutherland D,
1048 Pielot R, Smalla KH, Tang H, Tashman K, Toonen RFG, Verpelli C, Reig-Viader R, Watanabe K, van
1049 Weering J, Achsel T, Ashrafi G, Asi N, Brown TC, De Camilli P, Feuermann M, Foulger RE, Gaudet P,
1050 Joglekar A, Kanellopoulos A, Malenka R, Nicoll RA, Pulido C, de Juan-Sanz J, Sheng M, Südhof TC,
1051 Tilgner HU, Bagni C, Bayés À, Biederer T, Brose N, Chua JJE, Dieterich DC, Gundelfinger ED,

1052 Hoogenraad C, Huganir RL, Jahn R, Kaeser PS, Kim E, Kreutz MR, McPherson PS, Neale BM,
 1053 O'Connor V, Posthuma D, Ryan TA, Sala C, Feng G, Hyman SE, Thomas PD, Smit AB, Verhage M.
 1054 2019. SynGO: An Evidence-Based, Expert-Curated Knowledge Base for the Synapse. *Neuron*
 1055 **103**:217-234.e4. doi:10.1016/j.neuron.2019.05.002

1056 Koster KP, Flores-Barrera E, De La Villarmois EA, Nguyen TTA, Niquila A, Noriega-González LY, Fyke Z,
 1057 Caballero A, Cologna SM, Tseng KY, Yoshii A. 2021. Loss of Depalmitoylation Exaggerates Synaptic
 1058 Upscaling and Leads to Neuroinflammation in a Lysosomal Storage Disease. *bioRxiv*
 1059 2021.12.16.473002. doi:10.1101/2021.12.16.473002

1060 Koster KP, Yoshii A. 2019. Depalmitoylation by palmitoyl-protein thioesterase 1 in neuronal health and
 1061 degeneration. *Frontiers in Synaptic Neuroscience* **11**:25. doi:10.3389/fnsyn.2019.00025

1062 Kouskou M, Thomson DM, Brett RR, Wheeler L, Tate RJ, Pratt JA, Chamberlain LH. 2018. Disruption of
 1063 the Zdhhc9 intellectual disability gene leads to behavioural abnormalities in a mouse model.
 1064 *Experimental Neurology* **308**:35–46. doi:10.1016/J.EXPNEUROL.2018.06.014

1065 Kuleshov M V., Jones MR, Rouillard AD, Fernandez NF, Duan Q, Wang Z, Koplev S, Jenkins SL, Jagodnik
 1066 KM, Lachmann A, McDermott MG, Monteiro CD, Gundersen GW, Ma'ayan A. 2016. Enrichr: a
 1067 comprehensive gene set enrichment analysis web server 2016 update. *Nucleic acids research*
 1068 **44**:W90–W97. doi:10.1093/nar/gkw377

1069 László ZI, Lele Z, Zöldi M, Miczán V, Mógor F, Simon GM, Mackie K, Kacs Kovics I, Cravatt BF, Katona I.
 1070 2020. ABHD4-dependent developmental anoikis safeguards the embryonic brain. *Nature*
 1071 *Communications* **11**. doi:10.1038/s41467-020-18175-4

1072 Lemonidis K, Sanchez-Perez MC, Chamberlain LH. 2015. Identification of a novel sequence motif
 1073 recognized by the ankyrin repeat domain of zDHC17/13 S-acyltransferases. *Journal of Biological*
 1074 *Chemistry* **290**:21939–21950. doi:10.1074/jbc.M115.657668

1075 Lin DTS, Conibear E. 2015. ABHD17 proteins are novel protein depalmitoylases that regulate N-Ras
 1076 palmitate turnover and subcellular localization. *eLife* **4**. doi:10.7554/eLife.11306

1077 Lin DTS, Davis NG, Conibear E. 2017. Targeting the Ras palmitoylation/depalmitoylation cycle in cancer.
 1078 *Biochemical Society Transactions* **45**:913–921. doi:10.1042/BST20160303

1079 Lu JY, Verkruyse LA, Hofmann SL. 1996. Lipid thioesters derived from acylated proteins accumulate in

1080 infantile neuronal ceroid lipofuscinosis: Correction of the defect in lymphoblasts by recombinant
1081 palmitoyl-protein thioesterase. *Proceedings of the National Academy of Sciences of the United*
1082 *States of America* **93**:10046–10050. doi:10.1073/pnas.93.19.10046

1083 Ma Y, Liu H, Ou Z, Qi C, Xing R, Wang S, Han Y, Zhao T-J, Chen Y. 2021. DHHC5 facilitates oligodendrocyte
1084 development by palmitoylating and activating STAT3. *Glia*. doi:10.1002/glia.24113

1085 Malgapo MIP, Linder ME. 2021. Substrate recruitment by zDHHC protein acyltransferases. *Open Biology*
1086 **11**:rsob.210026. doi:10.1098/rsob.210026

1087 Marques S, Zeisel A, Codeluppi S, Van Bruggen D, Falcão AM, Xiao L, Li H, Häring M, Hochgerner H,
1088 Romanov RA, Gyllborg D, Muñoz-Manchado AB, La Manno G, Lönnerberg P, Floriddia EM, Rezayee
1089 F, Ernfors P, Arenas E, Hjerling-Leffler J, Harkany T, Richardson WD, Linnarsson S, Castelo-Branco G.
1090 2016. Oligodendrocyte heterogeneity in the mouse juvenile and adult central nervous system.
1091 *Science* **352**:1326–1329. doi:10.1126/science.aaf6463

1092 Matt L, Kim K, Chowdhury D, Hell JW. 2019. Role of palmitoylation of postsynaptic proteins in promoting
1093 synaptic plasticity. *Frontiers in Molecular Neuroscience*. doi:10.3389/fnmol.2019.00008

1094 Mi H, Dong Q, Muruganujan A, Gaudet P, Lewis S, Thomas PD. 2009. PANTHER version 7: Improved
1095 phylogenetic trees, orthologs and collaboration with the Gene Ontology Consortium. *Nucleic Acids*
1096 *Research* **38**. doi:10.1093/nar/gkp1019

1097 Mitchell DA, Hamel LD, Reddy KD, Farh L, Rettew LM, Sanchez PR, Deschenes RJ. 2014. Mutations in the
1098 X-linked intellectual disability gene, zDHHC9, alter autopalmitylation activity by distinct
1099 mechanisms. *Journal of Biological Chemistry* **289**:18582–18592. doi:10.1074/jbc.M114.567420

1100 Mukai J, Liu H, Burt RA, Swor DE, Lai WS, Karayiorgou M, Gogos JA. 2004. Evidence that the gene
1101 encoding ZDHHC8 contributes to the risk of schizophrenia. *Nature Genetics* **36**:725–731.
1102 doi:10.1038/ng1375

1103 Nita DA, Mole SE, Minassian BA. 2016. Neuronal ceroid lipofuscinoses. *Epileptic Disorders* **18**:S73–S88.
1104 doi:10.1684/epd.2016.0844

1105 Pitts MW, Hoffmann PR. 2018. Endoplasmic reticulum-resident selenoproteins as regulators of calcium
1106 signaling and homeostasis. *Cell Calcium* **70**:76–86. doi:10.1016/j.ceca.2017.05.001

1107 Plain F, Howie J, Kennedy J, Brown E, Shattock MJ, Fraser NJ, Fuller W. 2020. Control of protein

1108 palmitoylation by regulating substrate recruitment to a zDHHC-protein acyltransferase.
 1109 *Communications Biology* **3**:1–10. doi:10.1038/s42003-020-01145-3

1110 Rana MS, Lee CJ, Banerjee A. 2018. The molecular mechanism of DHHC protein acyltransferases.
 1111 *Biochemical Society Transactions* **47**:157–167. doi:10.1042/BST20180429

1112 Raymond FL, Tarpey PS, Edkins S, Tofts C, O’Meara S, Teague J, Butler A, Stevens C, Barthorpe S, Buck G,
 1113 Cole J, Dicks E, Gray K, Halliday K, Hills K, Hinton J, Jones D, Menzies A, Perry J, Raine K, Shepherd R,
 1114 Small A, Varian J, Widaa S, Mallya U, Moon J, Luo Y, Shaw M, Boyle J, Kerr B, Turner G, Quarrell O,
 1115 Cole T, Easton DF, Wooster R, Bobrow M, Schwartz CE, Gecz J, Stratton MR, Futreal PA. 2007.
 1116 Mutations in ZDHHC9, Which Encodes a Palmitoyltransferase of NRAS and HRAS, Cause X-Linked
 1117 Mental Retardation Associated with a Marfanoid Habitus. *The American Journal of Human Genetics*
 1118 **80**:982–987. doi:10.1086/513609

1119 Roberts MS, Macauley SL, Wong AM, Yilmaz D, Hohm S, Cooper JD, Sands MS. 2012. Combination small
 1120 molecule PPT1 mimetic and CNS-directed gene therapy as a treatment for infantile neuronal ceroid
 1121 lipofuscinosis. *Journal of Inherited Metabolic Disease* **35**:847–857. doi:10.1007/s10545-011-9446-x

1122 Rocks O, Gerauer M, Vartak N, Koch S, Huang ZP, Pechlivanis M, Kuhlmann J, Brunsveld L, Chandra A,
 1123 Ellinger B, Waldmann H, Bastiaens PIH. 2010. The palmitoylation machinery is a spatially organizing
 1124 system for peripheral membrane proteins. *Cell* **141**:458–471. doi:10.1016/j.cell.2010.04.007

1125 Rodenburg RNP, Snijder J, Van De Waterbeemd M, Schouten A, Granneman J, Heck AJR, Gros P. 2017.
 1126 Stochastic palmitoylation of accessible cysteines in membrane proteins revealed by native mass
 1127 spectrometry. *Nature Communications* **8**:1–9. doi:10.1038/s41467-017-01461-z

1128 Rosenberg AB, Roco CM, Muscat RA, Kuchina A, Sample P, Yao Z, Graybuck LT, Peeler DJ, Mukherjee S,
 1129 Chen W, Pun SH, Sellers DL, Tasic B, Seelig G. 2018. Single-cell profiling of the developing mouse
 1130 brain and spinal cord with split-pool barcoding. *Science* **360**:176–182.
 1131 doi:10.1126/science.aam8999

1132 Salaun C, Locatelli C, Zmuda F, González JC, Chamberlain LH. 2020. Accessory proteins of the zDHHC
 1133 family of S-acylation enzymes. *Journal of Cell Science* **133**. doi:10.1242/jcs.251819

1134 Sanders SS, Martin DDO, Butland SL, Lavallée-Adam M, Calzolari D, Kay C, Yates JR, Hayden MR. 2015.
 1135 Curation of the Mammalian Palmitoylome Indicates a Pivotal Role for Palmitoylation in Diseases
 1136 and Disorders of the Nervous System and Cancers. *PLoS Computational Biology* **11**:e1004405.

doi:10.1371/journal.pcbi.1004405

Saunders A, Macosko EZ, Wysoker A, Goldman M, Krienen FM, de Rivera H, Bien E, Baum M, Bortolin L, Wang S, Goeva A, Nemesh J, Kamitaki N, Brumbaugh S, Kulp D, McCarroll SA. 2018. Molecular Diversity and Specializations among the Cells of the Adult Mouse Brain. *Cell* **174**:1015-1030.e16. doi:10.1016/j.cell.2018.07.028

Schneider A, Länder H, Schulz G, Wolburg H, Nave K-A, Schulz JB, Simons M. 2005. Palmitoylation is a sorting determinant for transport to the myelin membrane. *Journal of cell science* **118**:2415–23. doi:10.1242/jcs.02365

Schwarz F, Aepli M. 2011. Mechanisms and principles of N-linked protein glycosylation. *Current Opinion in Structural Biology* **21**:576–582. doi:10.1016/j.sbi.2011.08.005

Sharma K, Schmitt S, Bergner CG, Tyanova S, Kannaiyan N, Manrique-Hoyos N, Kongi K, Cantuti L, Hanisch UK, Philips MA, Rossner MJ, Mann M, Simons M. 2015. Cell type- and brain region-resolved mouse brain proteome. *Nature Neuroscience* **18**:1819–1831. doi:10.1038/nn.4160

Shimell JJ, Shah BS, Cain SM, Thouta S, Kuhlmann N, Tatarnikov I, Jovellar DB, Brigidi GS, Kass J, Milnerwood AJ, Snutch TP, Bamji SX. 2019. The X-Linked Intellectual Disability Gene *Zdhc9* Is Essential for Dendrite Outgrowth and Inhibitory Synapse Formation. *Cell Reports* **29**:2422-2437.e8. doi:10.1016/j.celrep.2019.10.065

Shyng C, Nelvagal HR, Dearborn JT, Tyynelä J, Schmidt RE, Sands MS, Cooper JD. 2017. Synergistic effects of treating the spinal cord and brain in CLN1 disease. *Proceedings of the National Academy of Sciences of the United States of America* **114**:E5920–E5929. doi:10.1073/pnas.1701832114

Simon GM, Cravatt BF. 2010. Activity-based proteomics of enzyme superfamilies: Serine hydrolases as a case study. *Journal of Biological Chemistry*. doi:10.1074/jbc.R109.097600

Sjöstedt E, Zhong W, Fagerberg L, Karlsson M, Mitsios N, Adori C, Oksvold P, Edfors F, Limiszewska A, Hikmet F, Huang J, Du Y, Lin L, Dong Z, Yang L, Liu X, Jiang H, Xu X, Wang J, Yang H, Bolund L, Mardinoglu A, Zhang C, von Feilitzen K, Lindskog C, Pontén F, Luo Y, Hökfelt T, Uhlén M, Mulder J. 2020. An atlas of the protein-coding genes in the human, pig, and mouse brain. *Science* **367**:eaay5947. doi:10.1126/science.aay5947

Solis GP, Kazemzadeh A, Abrami L, Valnohova J, Alvarez C, van der Goot FG, Katanaev VL. 2022. Local

1165 and substrate-specific S-palmitoylation determines subcellular localization of Gao. *Nature*
1166 *Communications* 2022 13:1 **13**:1–21. doi:10.1038/s41467-022-29685-8

1167 Swarthout JT, Lobo S, Farh L, Croke MR, Greentree WK, Deschenes RJ, Linder ME. 2005. DHHC9 and
1168 GCP16 constitute a human protein fatty acyltransferase with specificity for H- and N-Ras. *Journal of*
1169 *Biological Chemistry* **280**:31141–31148. doi:10.1074/jbc.M504113200

1170 Szklarczyk D, Gable AL, Lyon D, Junge A, Wyder S, Huerta-Cepas J, Simonovic M, Doncheva NT, Morris JH,
1171 Bork P, Jensen LJ, Von Mering C. 2019. STRING v11: Protein-protein association networks with
1172 increased coverage, supporting functional discovery in genome-wide experimental datasets.
1173 *Nucleic Acids Research* **47**:D607–D613. doi:10.1093/nar/gky1131

1174 Tasic B, Yao Z, Graybuck LT, Smith KA, Nguyen TN, Bertagnolli D, Goldy J, Garren E, Economo MN,
1175 Viswanathan S, Penn O, Bakken T, Menon V, Miller J, Fong O, Hirokawa KE, Lathia K, Rimorin C,
1176 Tieu M, Larsen R, Casper T, Barkan E, Kroll M, Parry S, Shapovalova N V., Hirschstein D, Pendergraft
1177 J, Sullivan HA, Kim TK, Szafer A, Dee N, Groblewski P, Wickersham I, Cetin A, Harris JA, Levi BP,
1178 Sunkin SM, Madisen L, Daigle TL, Looger L, Bernard A, Phillips J, Lein E, Hawrylycz M, Svoboda K,
1179 Jones AR, Koch C, Zeng H. 2018. Shared and distinct transcriptomic cell types across neocortical
1180 areas. *Nature* **563**:72–78. doi:10.1038/s41586-018-0654-5

1181 Thomas GM, Hayashi T, Chiu SL, Chen CM, Huganir RL. 2012. Palmitoylation by DHHC5/8 Targets GRIP1
1182 to Dendritic Endosomes to Regulate AMPA-R Trafficking. *Neuron* **73**:482–496.
1183 doi:10.1016/j.neuron.2011.11.021

1184 Thomas GM, Hayashi T, Huganir RL, Linden DJ. 2013. DHHC8-dependent PICK1 palmitoylation is required
1185 for induction of cerebellar long-term synaptic depression. *Journal of Neuroscience* **33**:15401–
1186 15407. doi:10.1523/JNEUROSCI.1283-13.2013

1187 Tzschach A, Grasshoff U, Beck-Woedl S, Dufke C, Bauer C, Kehrer M, Evers C, Moog U, Oehl-Jaschkowitz
1188 B, Donato N Di, Maiwald R, Jung C, Kuechler A, Schulz S, Meinecke P, Spranger S, Kohlhase J, Seidel
1189 J, Reif S, Rieger M, Riess A, Sturm M, Bickmann J, Schroeder C, Dufke A, Riess O, Bauer P. 2015.
1190 Next-generation sequencing in X-linked intellectual disability. *European Journal of Human Genetics*
1191 **23**:1513–1518. doi:10.1038/ejhg.2015.5

1192 Ubersax JA, Ferrell JE. 2007. Mechanisms of specificity in protein phosphorylation. *Nature Reviews*
1193 *Molecular Cell Biology* **8**:530–541. doi:10.1038/nrm2203

1194 Vartak N, Papke B, Grecco HE, Rossmannek L, Waldmann H, Hedberg C, Bastiaens PIH. 2014. The
1195 autodepalmitoylating activity of APT maintains the spatial organization of palmitoylated
1196 membrane proteins. *Biophysical Journal* **106**:93–105. doi:10.1016/j.bpj.2013.11.024

1197 Verardi R, Kim JS, Ghirlando R, Banerjee A. 2017. Structural Basis for Substrate Recognition by the
1198 Ankyrin Repeat Domain of Human DHHC17 Palmitoyltransferase. *Structure* **25**:1337–1347.e6.
1199 doi:10.1016/j.str.2017.06.018

1200 Virlogeux A, Scaramuzzino C, Lenoir S, Carpentier R, Louessard M, Genoux A, Lino P, Hinckelmann MV,
1201 Perrier AL, Humbert S, Saudou F. 2021. Increasing brain palmitoylation rescues behavior and
1202 neuropathology in Huntington disease mice. *Science Advances* **7**:799–830.
1203 doi:10.1126/sciadv.abb0799

1204 Vogel C, Marcotte EM. 2012. Insights into the regulation of protein abundance from proteomic and
1205 transcriptomic analyses. *Nature Reviews Genetics* **13**:227–232. doi:10.1038/nrg3185

1206 Wagstyl K, Ronan L, Whitaker KJ, Goodyer IM, Roberts N, Crow TJ, Fletcher PC. 2016. Multiple markers
1207 of cortical morphology reveal evidence of supragranular thinning in schizophrenia. *Translational*
1208 *Psychiatry* **6**:780. doi:10.1038/tp.2016.43

1209 Wilson RS, Nairn AC. 2018. Cell-type-specific proteomics: A neuroscience perspective. *Proteomes*.
1210 doi:10.3390/proteomes6040051

1211 Woodley KT, Collins MO. 2019. S-acylated Golga7b stabilises <scp>DHHC</scp> 5 at the plasma
1212 membrane to regulate cell adhesion. *EMBO reports* **20**:e47472. doi:10.15252/embr.201847472

1213 Yanai A, Huang K, Kang R, Singaraja RR, Arstikaitis P, Gan L, Orban PC, Mullard A, Cowan CM, Raymond
1214 LA, Drisdell RC, Green WN, Ravikumar B, Rubinsztein DC, El-Husseini A, Hayden MR. 2006.
1215 Palmitoylation of huntingtin by HIP14 is essential for its trafficking and function. *Nature*
1216 *Neuroscience* **9**:824–831. doi:10.1038/nn1702

1217 Yao Z, van Velthoven CTJ, Nguyen TN, Goldy J, Seden-Cortes AE, Baftizadeh F, Bertagnolli D, Casper T,
1218 Chiang M, Crichton K, Ding SL, Fong O, Garren E, Glandon A, Gouwens NW, Gray J, Graybuck LT,
1219 Hawrylycz MJ, Hirschstein D, Kroll M, Lathia K, Lee C, Levi B, McMillen D, Mok S, Pham T, Ren Q,
1220 Rimorin C, Shapovalova N, Sulc J, Sunkin SM, Tieu M, Torkelson A, Tung H, Ward K, Dee N, Smith
1221 KA, Tasic B, Zeng H. 2021. A taxonomy of transcriptomic cell types across the isocortex and
1222 hippocampal formation. *Cell* **184**:3222–3241.e26. doi:10.1016/j.cell.2021.04.021

1223 Yuan W, Lu L, Rao M, Huang Y, Liu CE, Liu S, Zhao Y, Liu H, Zhu J, Chao T, Wu C, Ren J, Lv L, Li W, Qi S,
 1224 Liang Y, Yue S, Gao J, Zhang Z, Kong E. 2021. GFAP hyperpalmitoylation exacerbates astrogliosis and
 1225 neurodegenerative pathology in PPT1-deficient mice. *Proceedings of the National Academy of*
 1226 *Sciences of the United States of America* **118**. doi:10.1073/pnas.2022261118

1227 Zareba-Kozioł M, Bartkowiak-Kaczmarek A, Figiel I, Krzystyniak A, Wojtowicz T, Bijata M, Włodarczyk J.
 1228 2019. Stress-induced Changes in the S-palmitoylation and S-nitrosylation of Synaptic Proteins.
 1229 *Molecular and Cellular Proteomics* **18**:1916–1938. doi:10.1074/mcp.RA119.001581

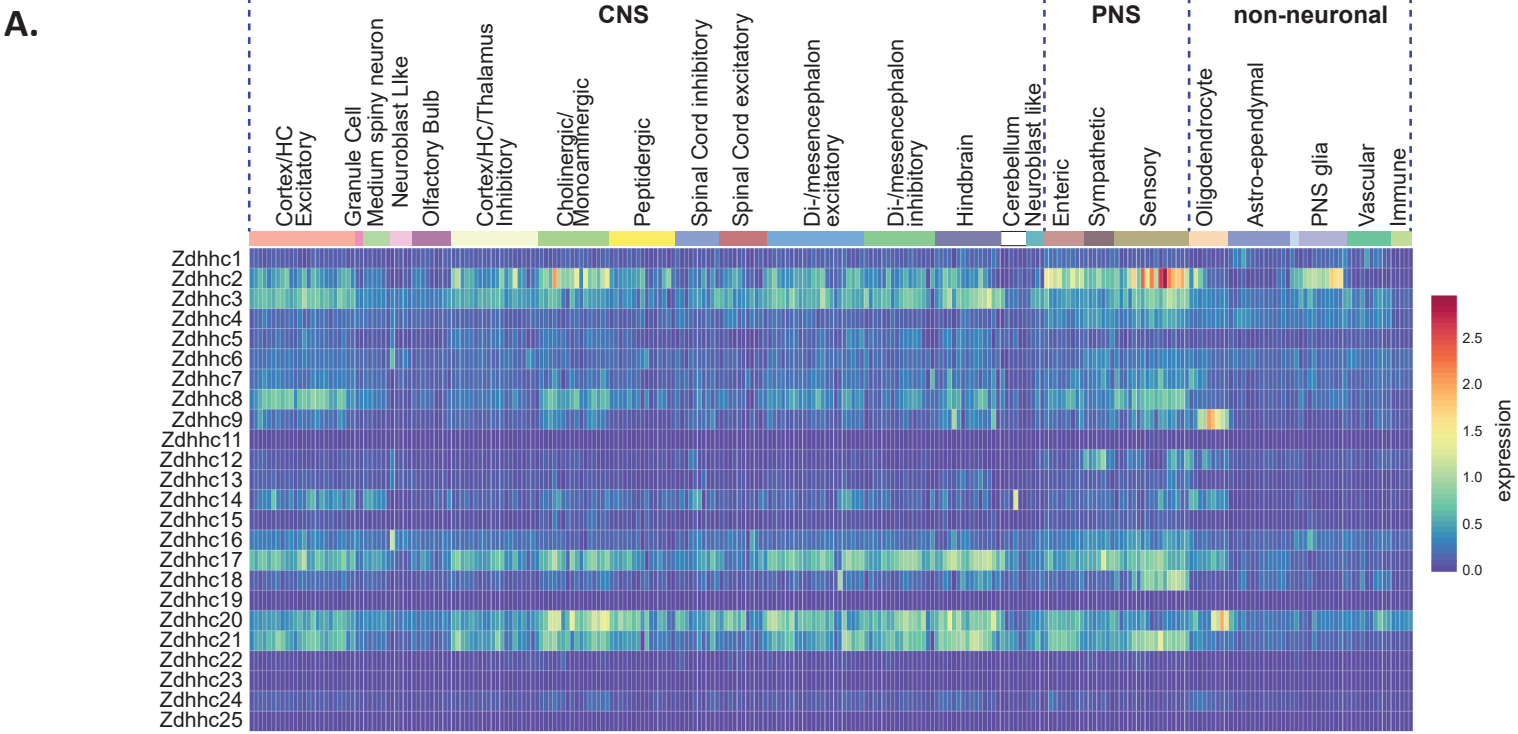
1230 Zeisel A, Hochgerner H, Lönnerberg P, Johnsson A, Memic F, van der Zwan J, Häring M, Braun E, Borm LE,
 1231 La Manno G, Codeluppi S, Furlan A, Lee K, Skene N, Harris KD, Hjerling-Leffler J, Arenas E, Ernfors P,
 1232 Marklund U, Linnarsson S. 2018. Molecular Architecture of the Mouse Nervous System. *Cell*
 1233 **174**:999-1014.e22. doi:10.1016/j.cell.2018.06.021

1234 Zeisel A, M̂oz-Manchado AB, Codeluppi S, Lönnerberg P, Manno G La, Juréus A, Marques S, Munguba H,
 1235 He L, Betsholtz C, Rolny C, Castelo-Branco G, Hjerling-Leffler J, Linnarsson S. 2015. Cell types in the
 1236 mouse cortex and hippocampus revealed by single-cell RNA-seq. *Science* **347**:1138–1142.
 1237 doi:10.1126/science.aaa1934

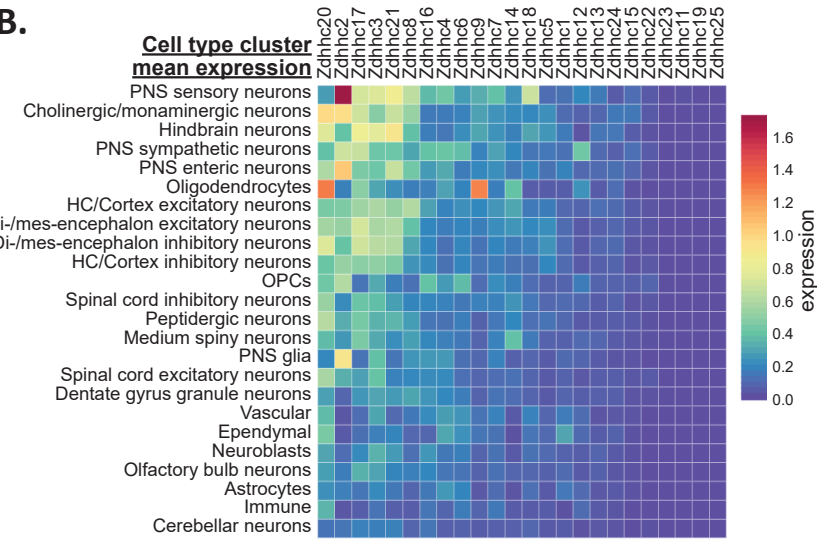
1238

Figure1

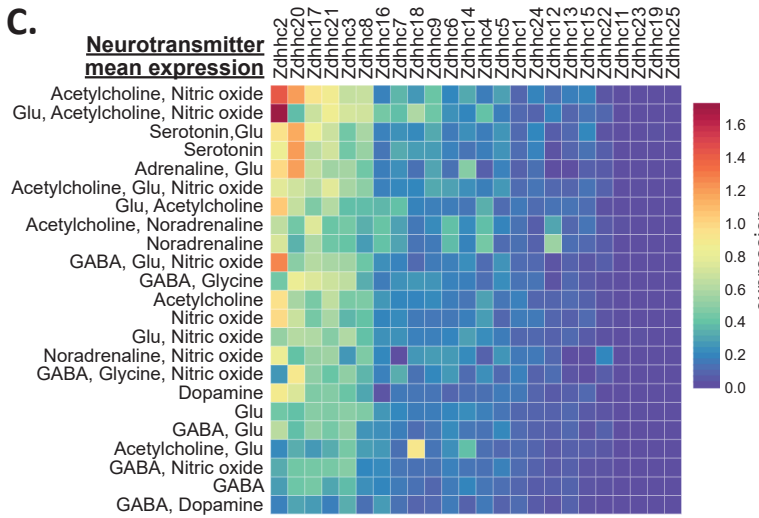
A.



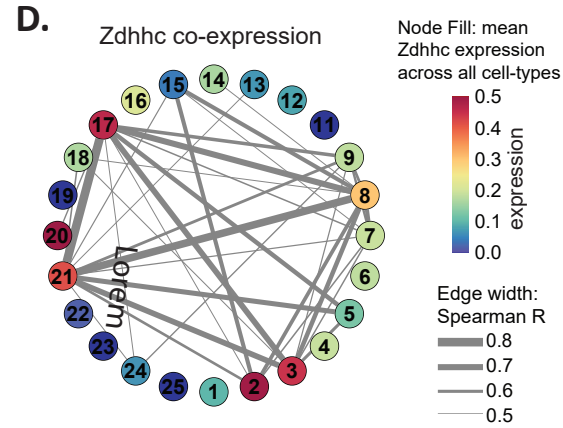
B.



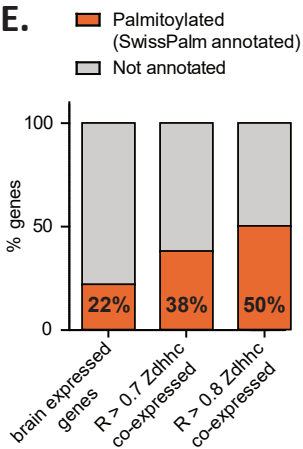
C.



D.



E.



F.

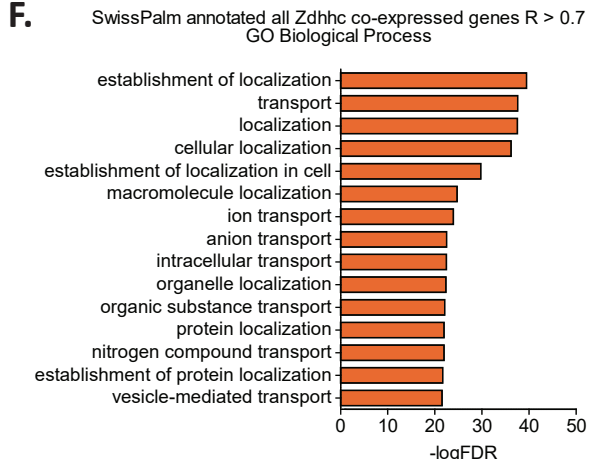


Figure 1-figure supplement 1

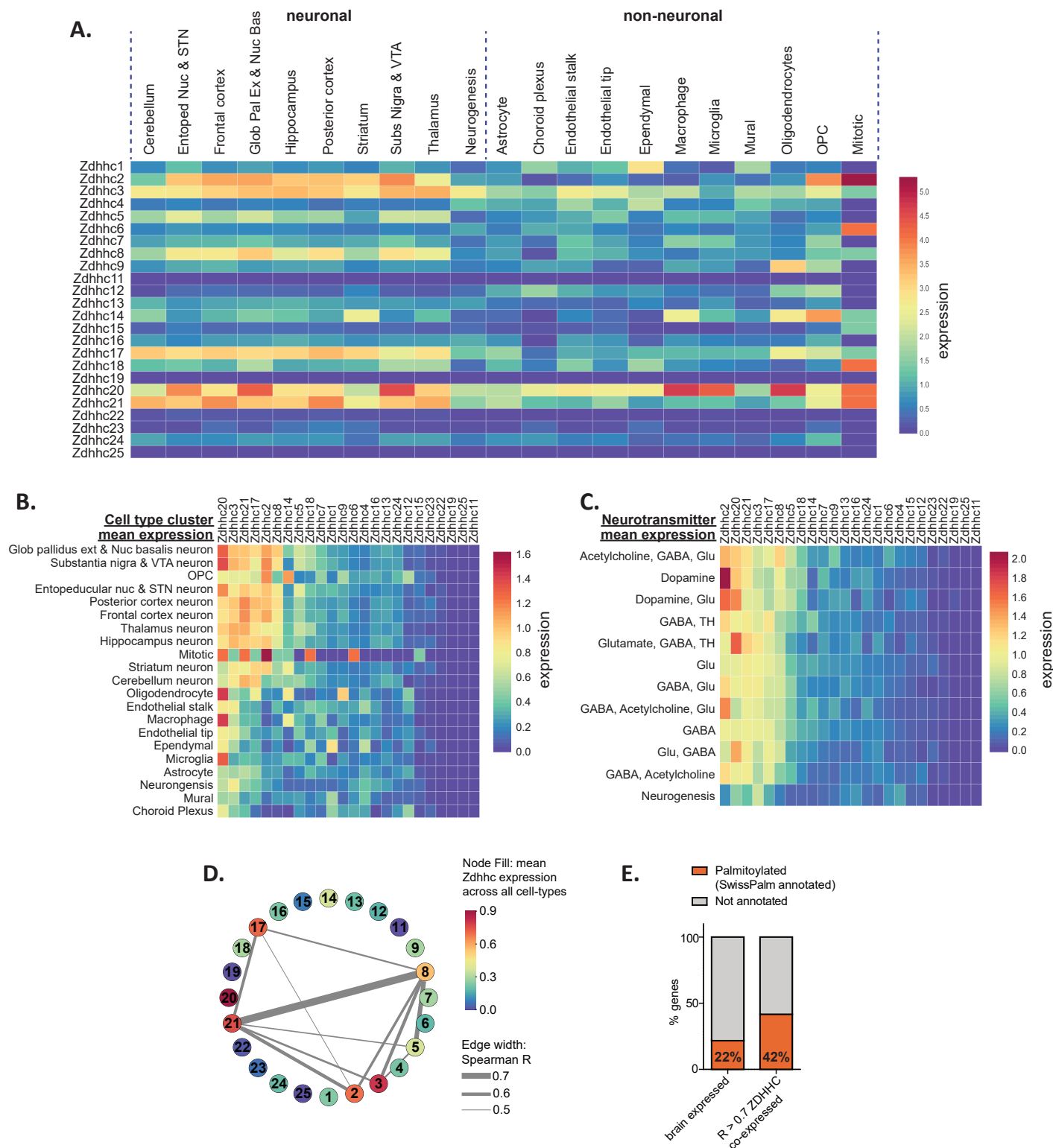


Figure 1-figure supplement 2

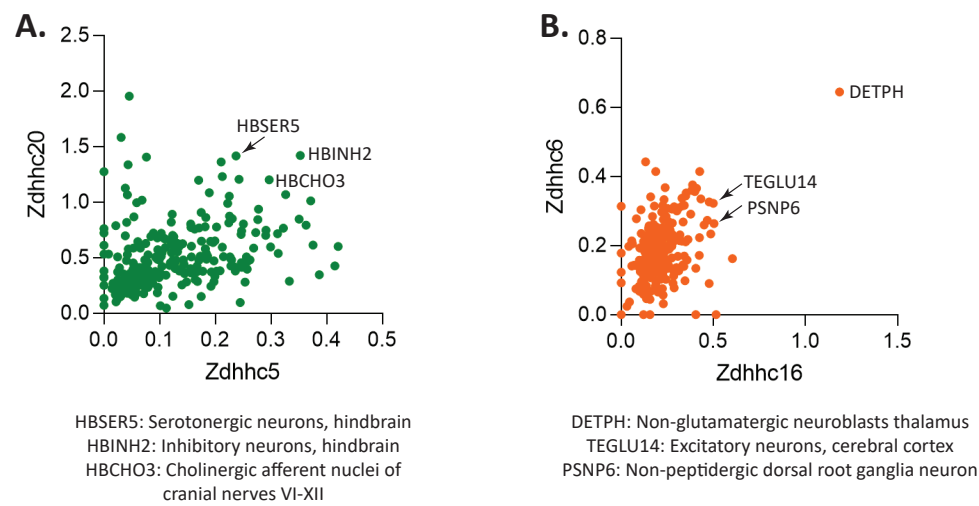


Figure 2

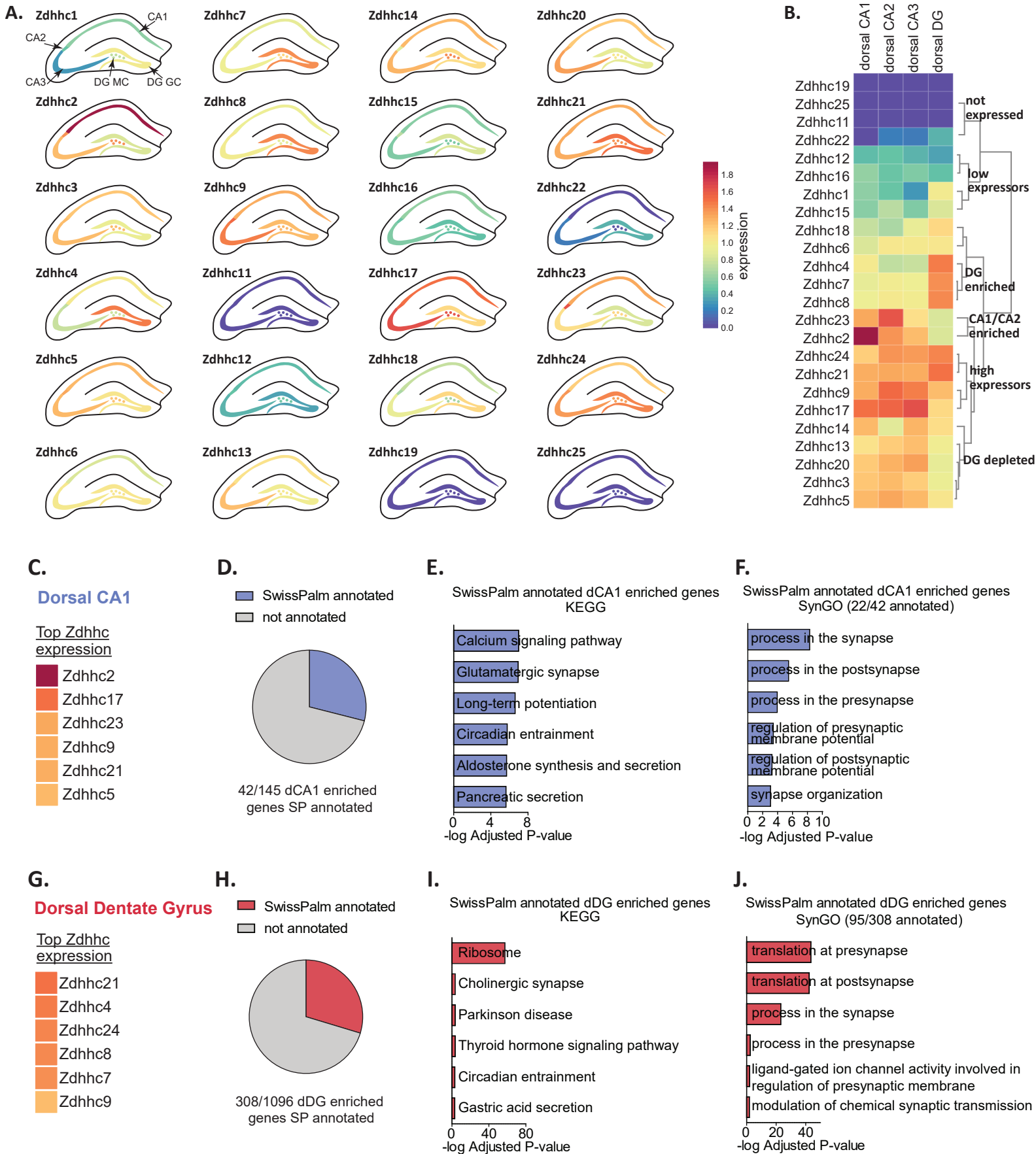


Figure 2-figure supplement 1

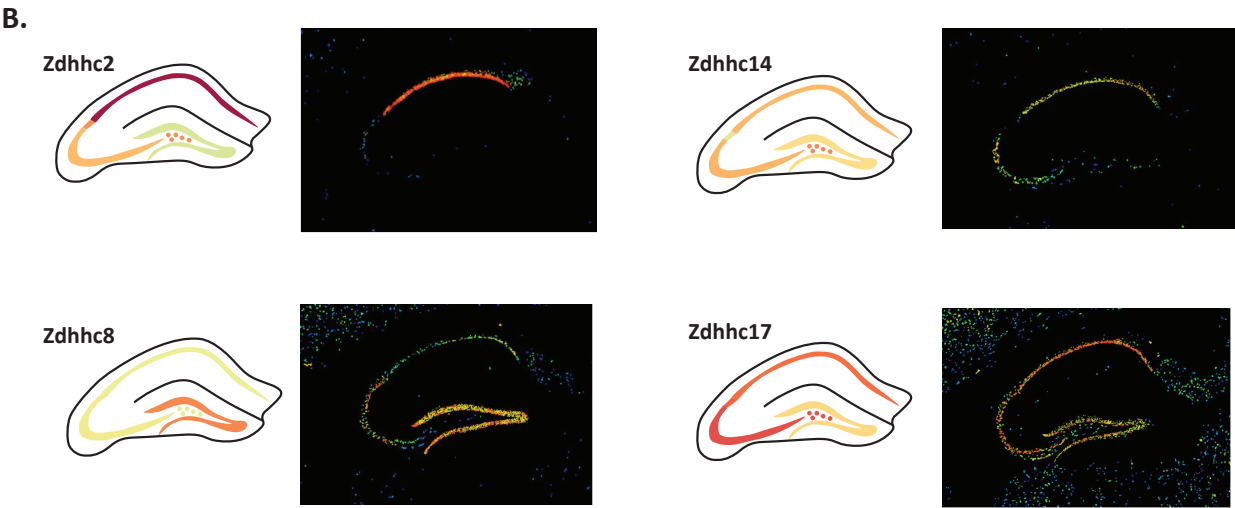
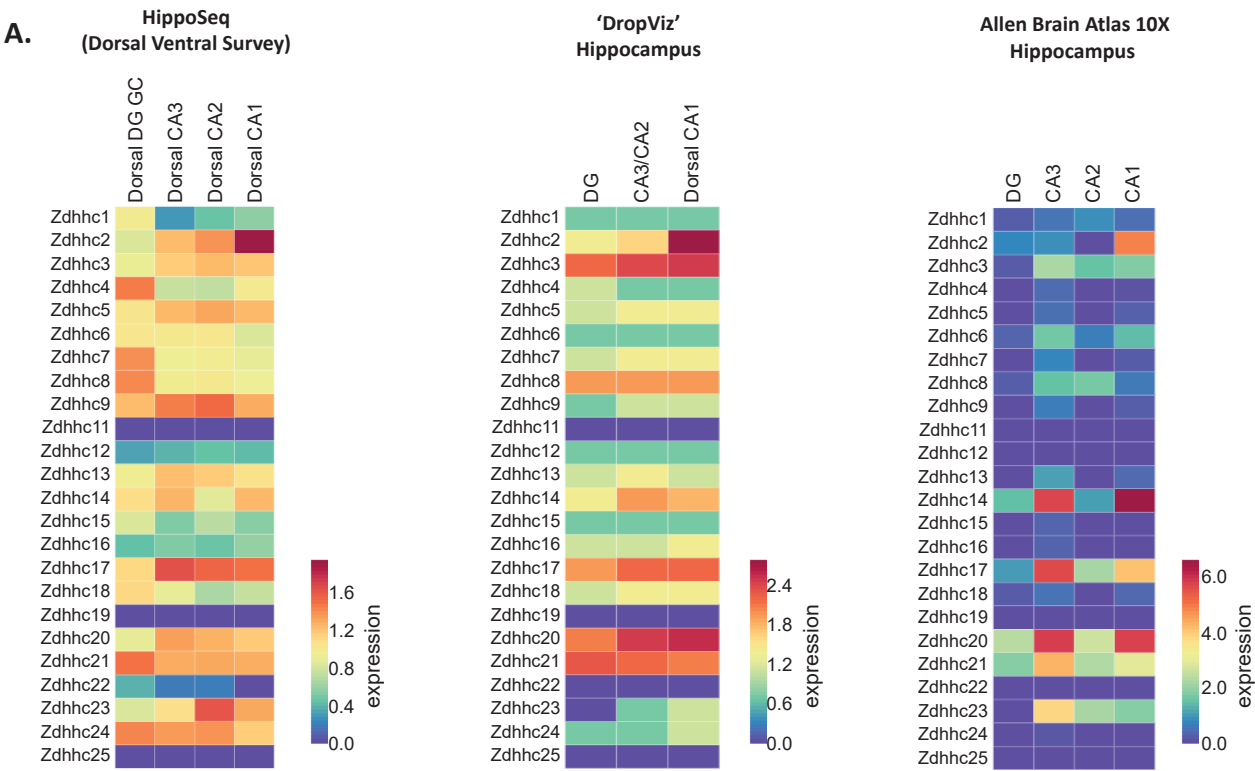
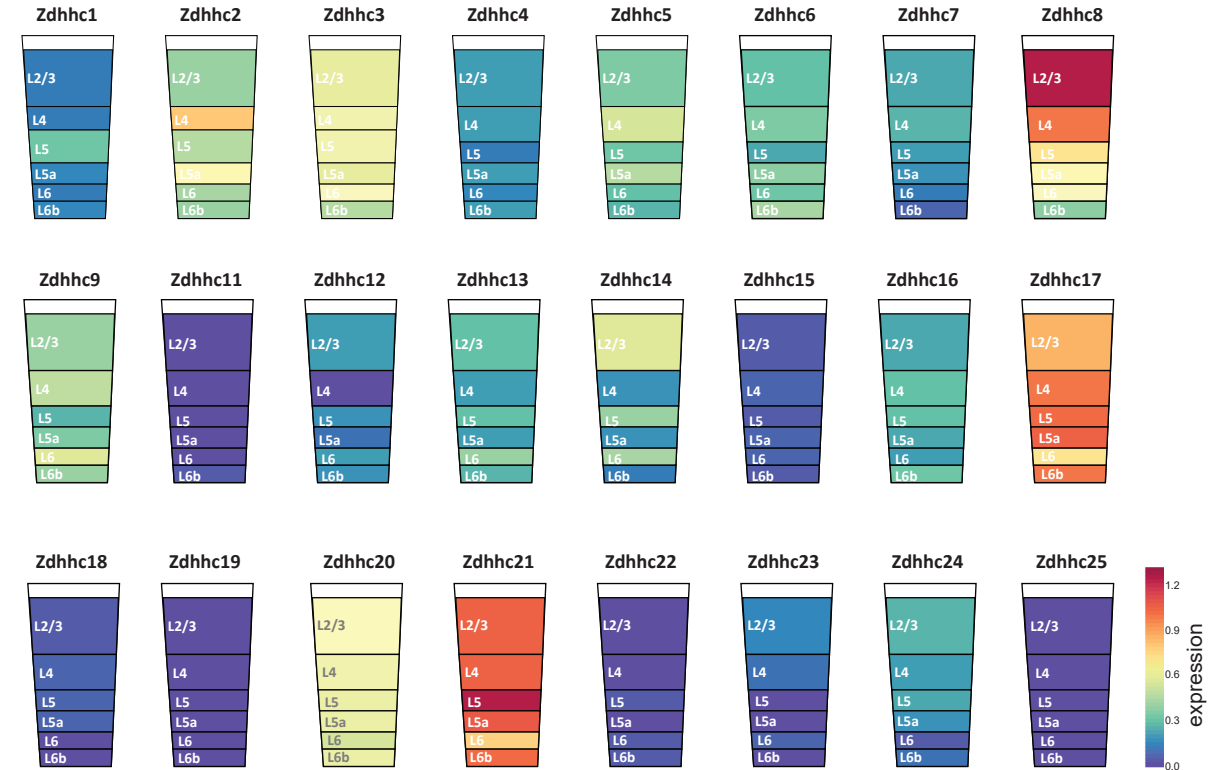


Figure 3

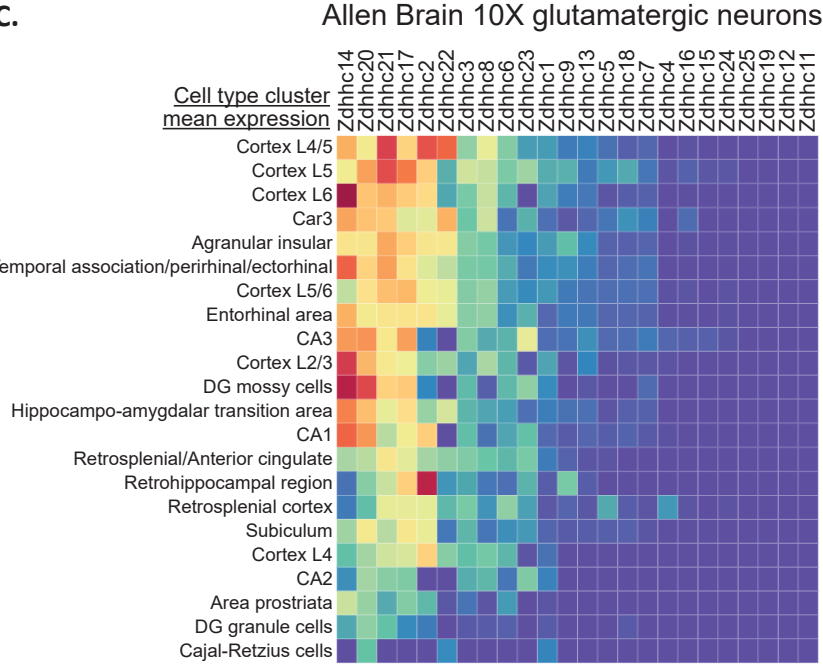
A.



B.



C.



D.

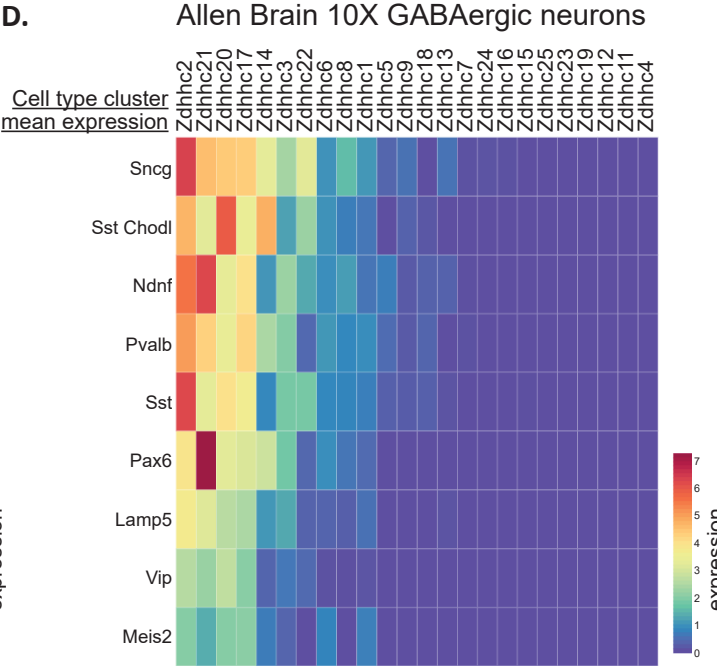


Figure 3-figure supplement 1

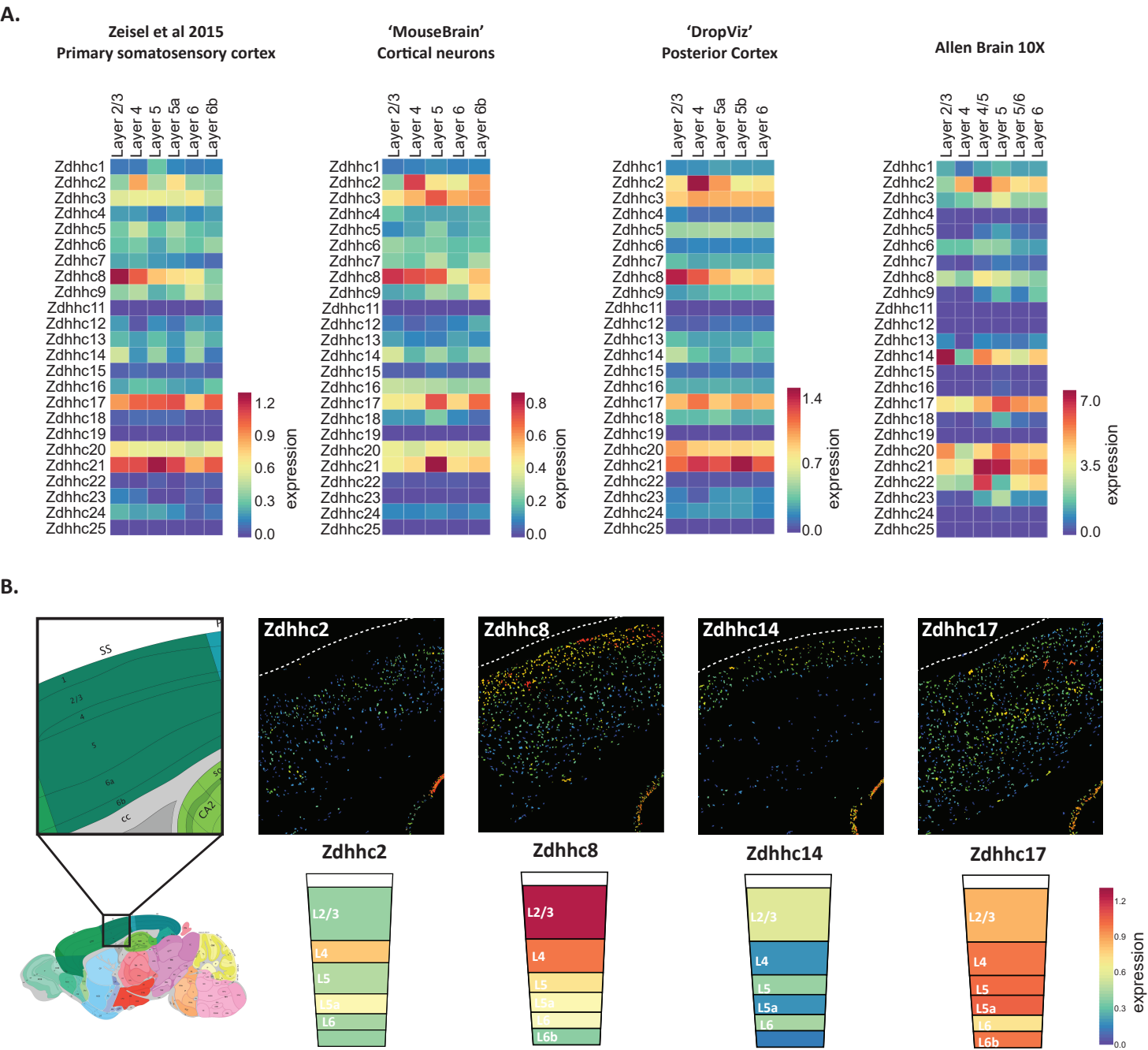


Figure 4

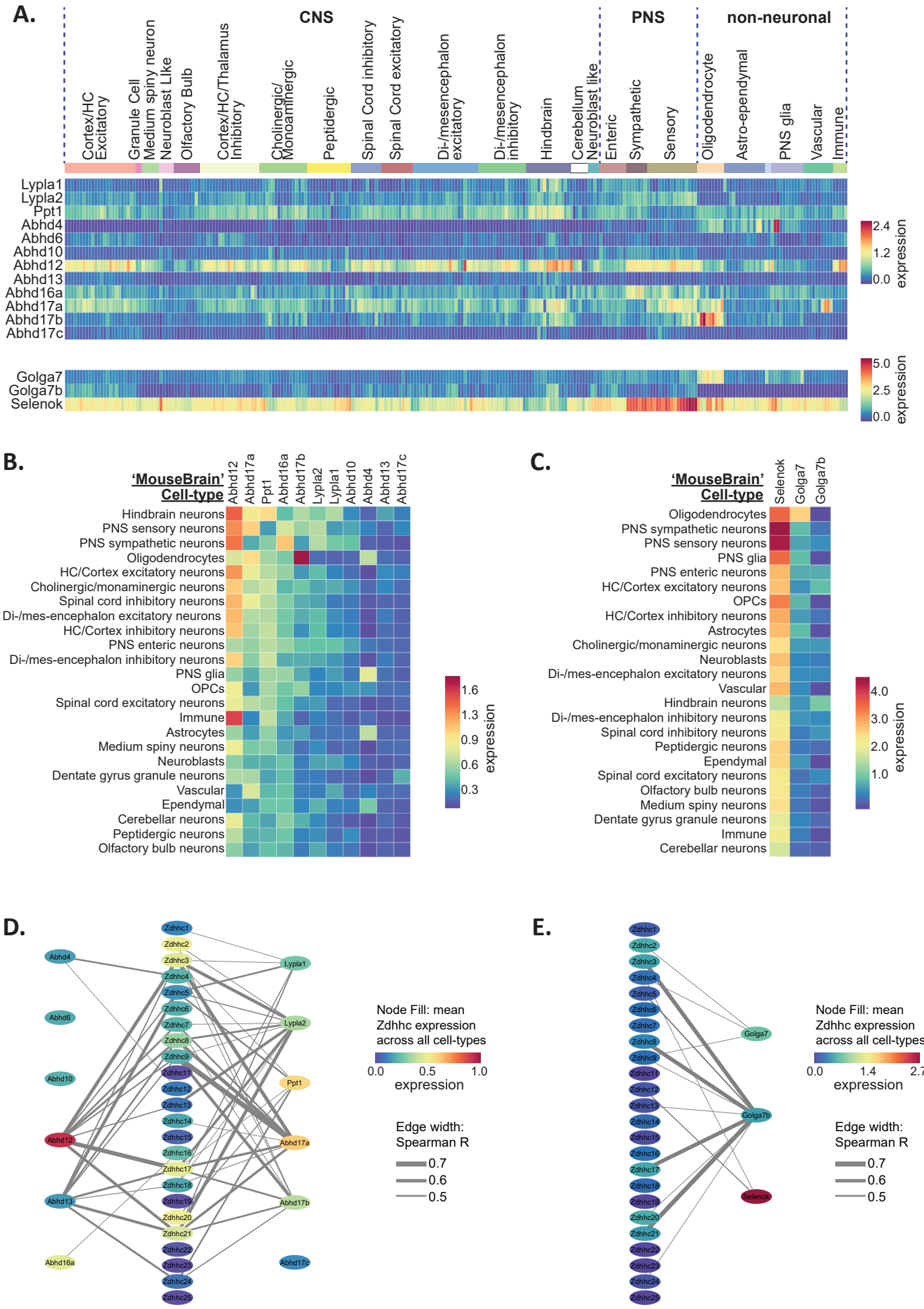


Figure 4-figure supplement 1

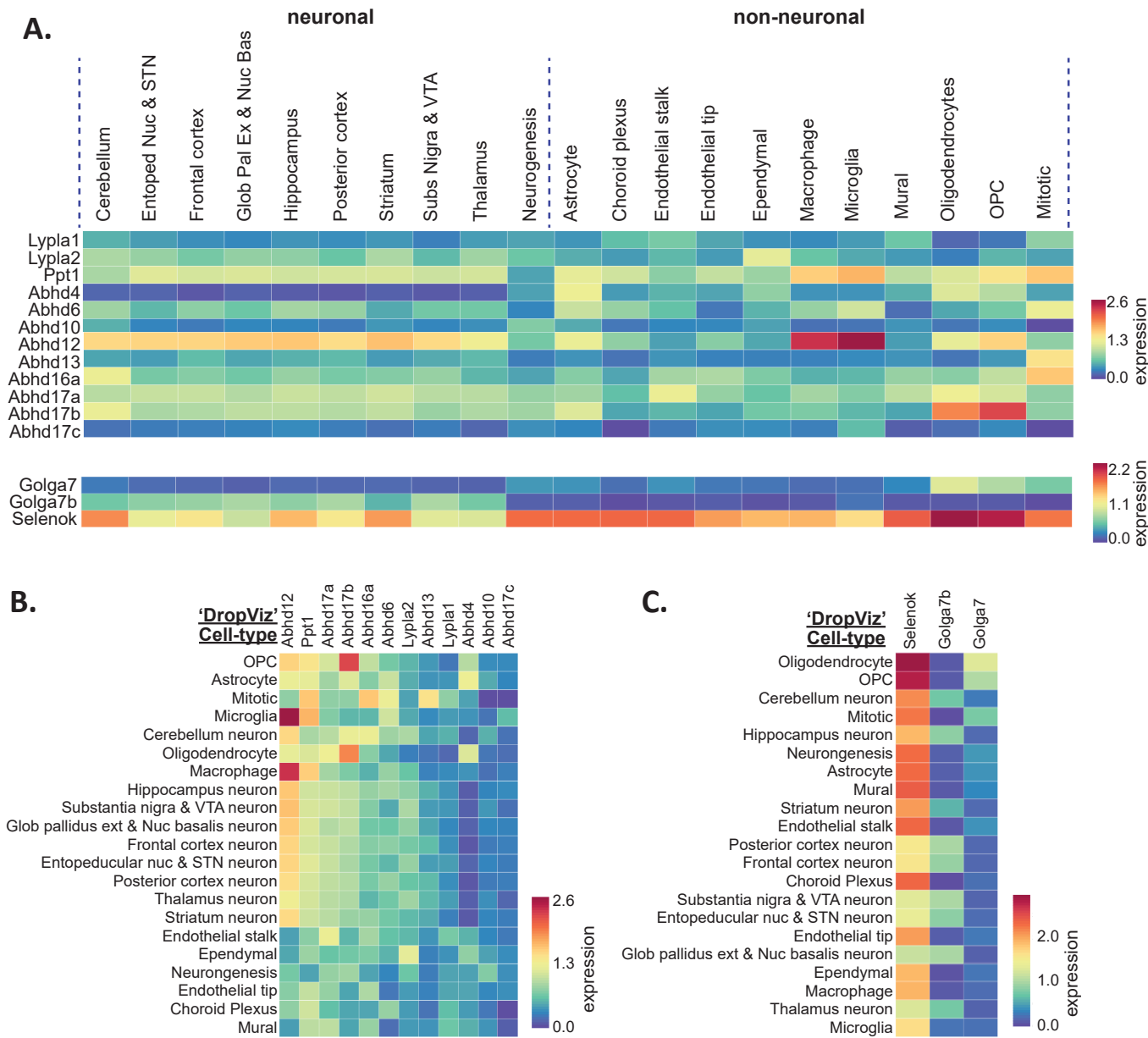


Figure 4-figure supplement 2

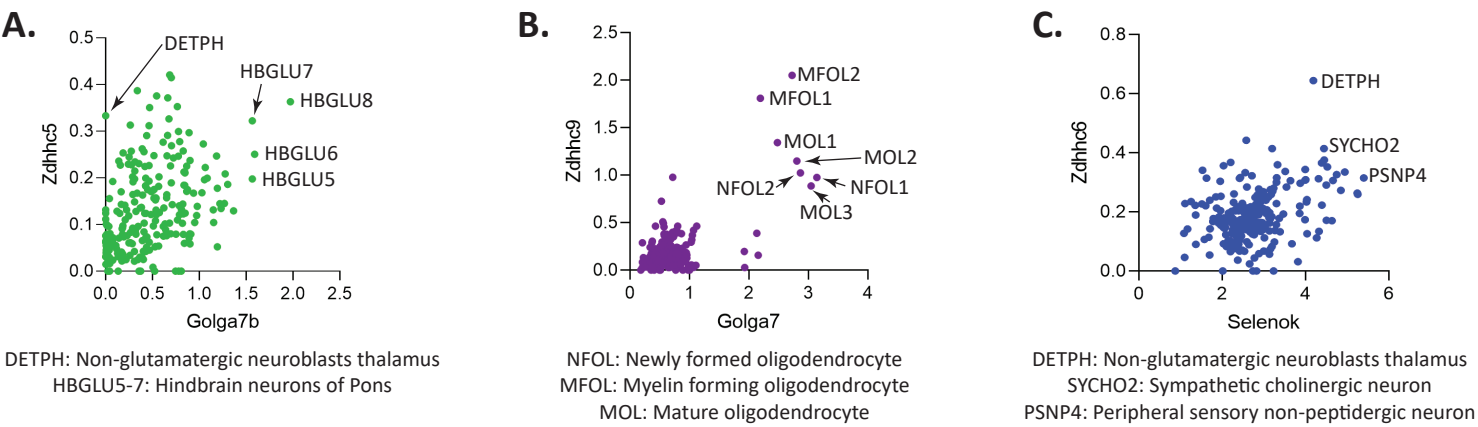


Figure 4-figure supplement 3

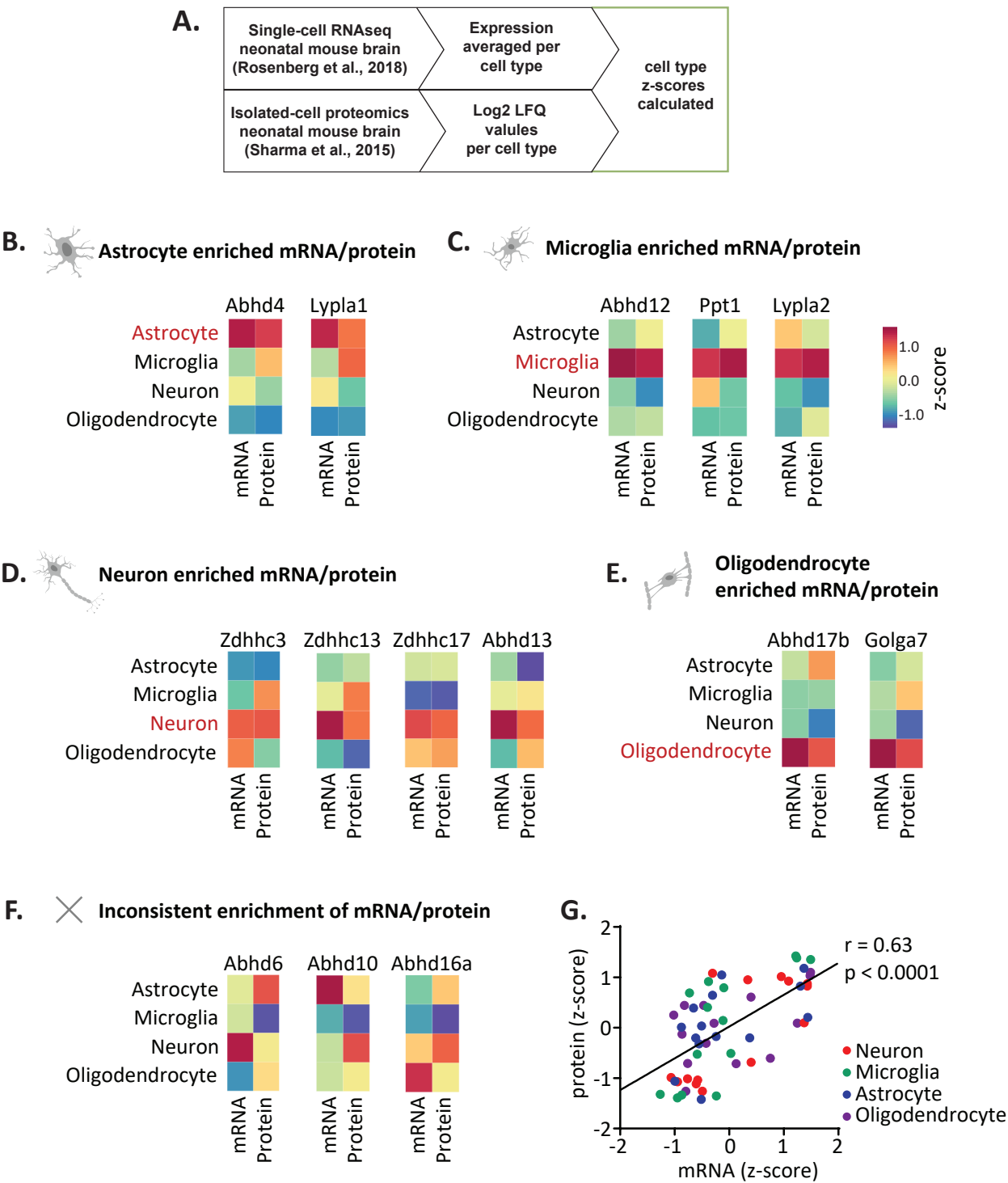


Figure 5

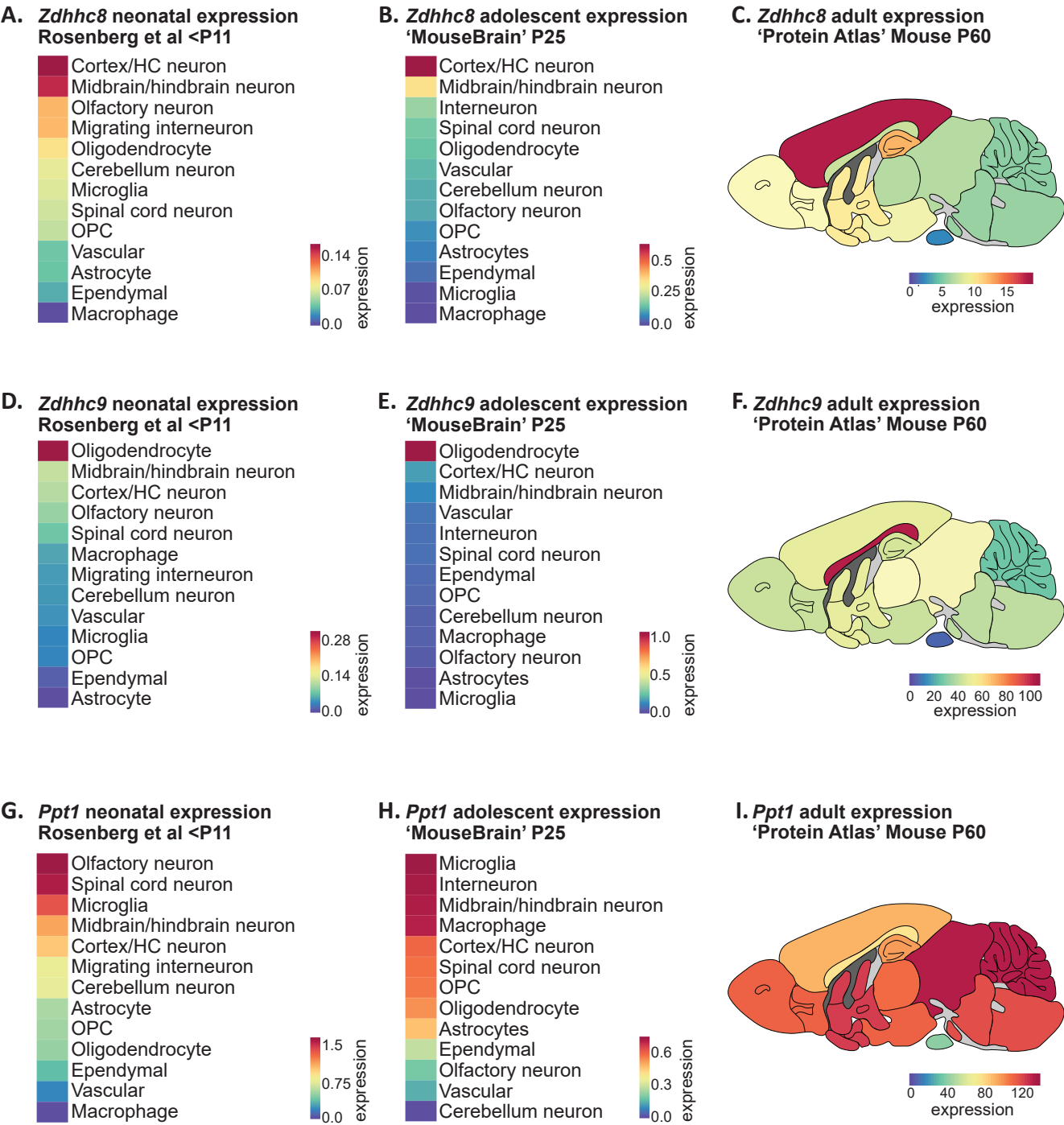


Figure 5-figure supplement 1

A.



□ Olfactory region
□ Cortex
□ Corpus Callosum
□ Basal Ganglia
□ Thalamus
□ Pituitary gland

□ Hippocampus
□ Hypothalamus
□ Midbrain
□ Cerebellum
□ Pons and medulla

Figure 6

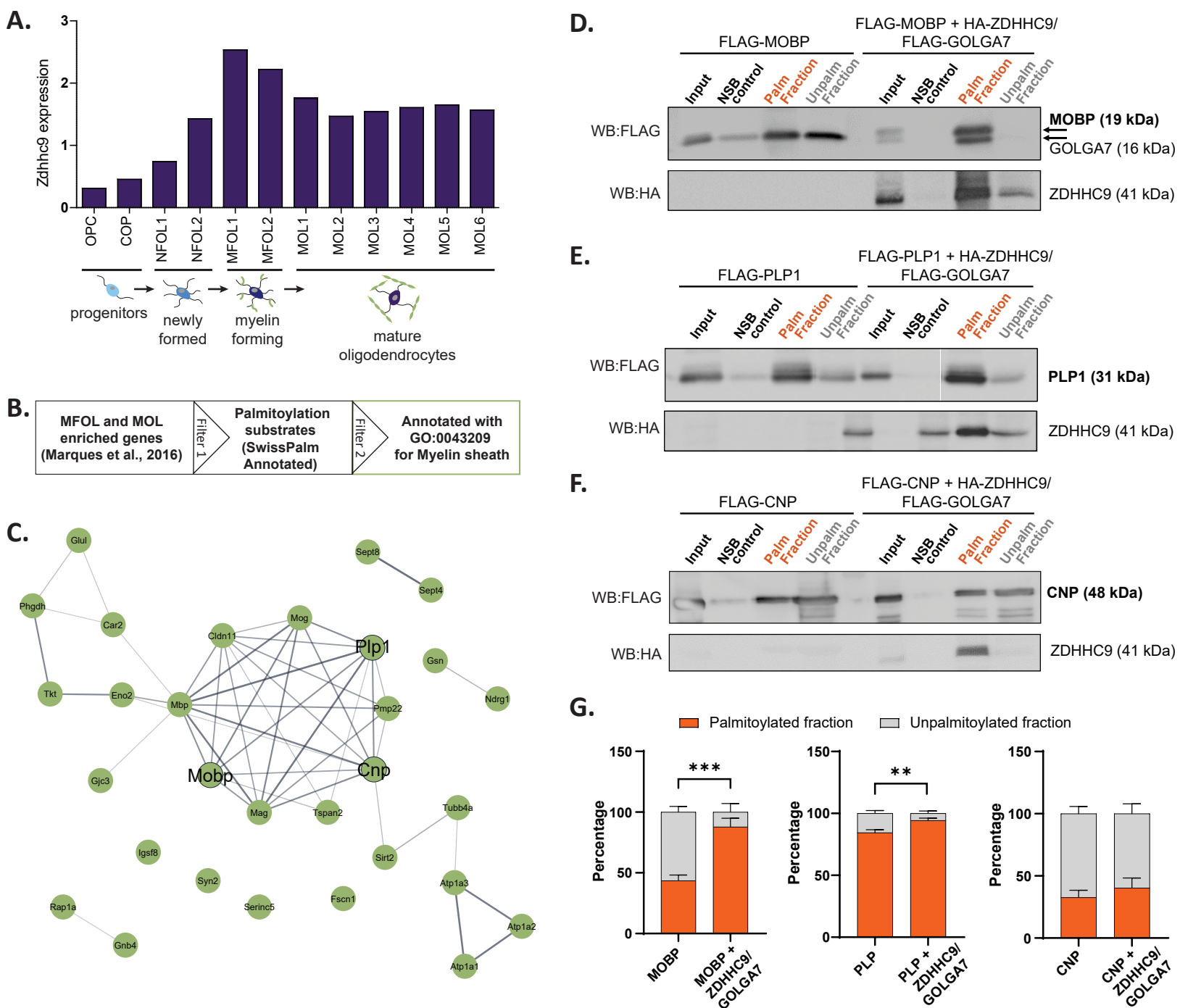
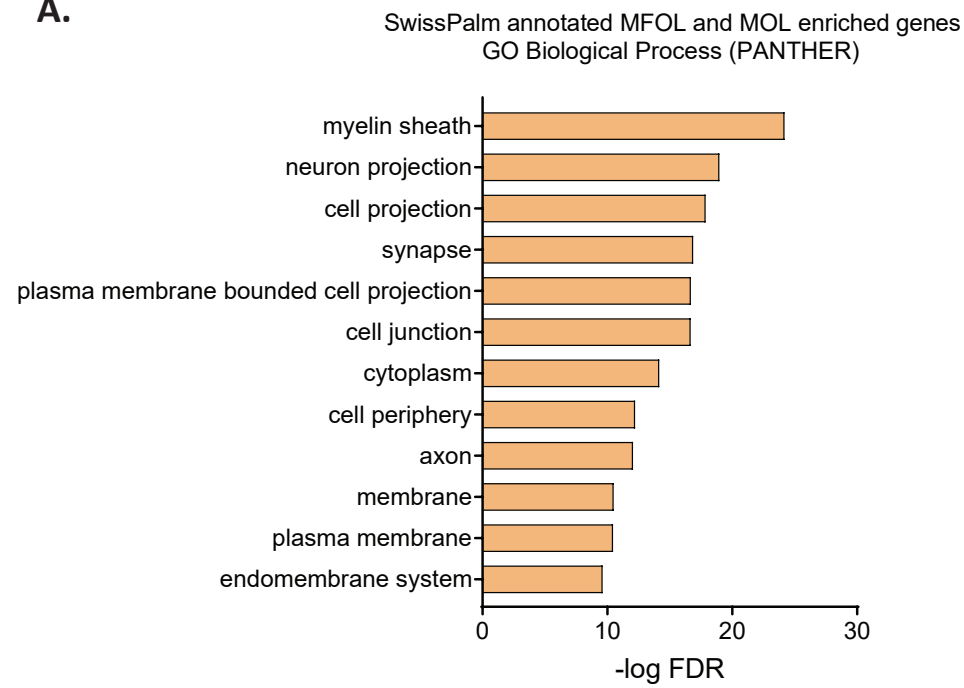
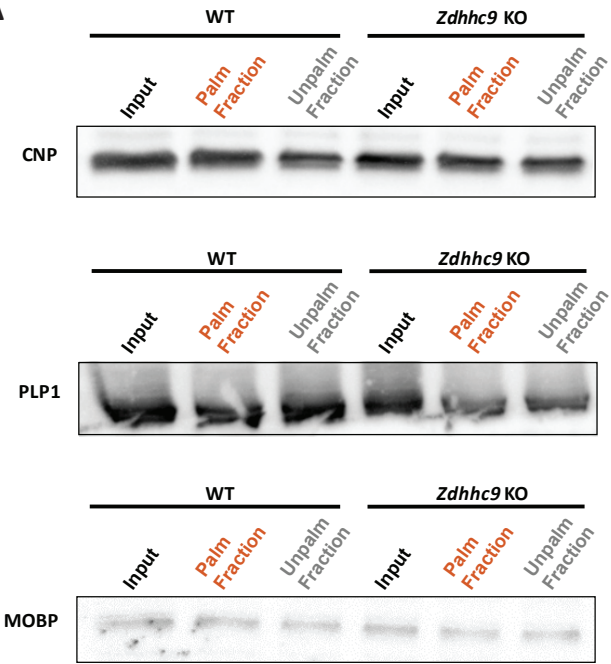


Figure 6-figure supplement 1

A.



A



B

